PHILOSOPHICAL TRANSACTIONS OF THE ROYAL SOCIETY A MATHEMATICAL, PHYSICAL & ENGINEERING SCIENCES

The Angular Acceleration of Liquid Helium. II

H. E. Hall

Phil. Trans. R. Soc. Lond. A 1957 **250**, 359-385
doi: 10.1098/rsta.1957.0024

THE ANGULAR ACCELERATION OF LIQUID HELIUM II

By H. E. HALL

The Royal Society Mond Laboratory, University of Cambridge

(*Communicated by D. Shoenberg, F.R.S.—Received 8 May 1957*)

[Plate 4]

CONTENTS

Direct measurements have been made of the torques required to produce angular acceleration and retardation of liquid helium II contained in a can filled with closely spaced disks at a temperature of 1·27°K. The acceleration and retardation processes are not equivalent, and it is suggested that this asymmetry is due to the presence of vortex lines in the uniformly rotating superfluid. It is found that the forces producing superfluid acceleration are dependent on the past history of the helium and are greatly enhanced if the disk surfaces are roughened; furthermore, the superfluid flow shows a strong tendency to be macroscopically irrotational during retardation. These properties suggest that the forces are associated with turbulence in the superfluid, and it is found that a consistent description of the results can be given in terms of a mutual friction due to such turbulence. Values of the mutual friction appropriate to a steady flow are deduced and found to be in good agreement with values deduced from the results of other isothermal flow experiments; they can be represented, above a critical velocity, by a modification of the law introduced by Gorter & Mellink (1949), namely

$$F_{sn} = A\rho_s\rho_n(|v_s - v_n| - v_0)^2\,(v_s - v_n),$$

with $A = 23 \pm 2$ poise^{-1}, $v_0 = -0{\cdot}6 \pm 0{\cdot}2$ cm s^{-1}. Below the critical velocity a persistent current with a lifetime of at least 25 min has been observed. In the last section quantitative results on the growth and decay of turbulence in a non-equilibrium situation are presented, and laws describing the growth and decay processes are formulated.

1. Introduction

By investigating the period and damping of oscillating disk systems in liquid helium II Hollis-Hallett (1952*a*) showed that the superfluid could be dragged into motion, but neither the force of mutual friction proposed by Gorter & Mellink (1949) to account for the results

of experiments on heat flow, nor any other force depending only on the relative velocity of the two fluids, was capable of accounting for the results. The object of the present experiments was to investigate the angular acceleration of the superfluid by a method capable of giving more detailed information than Hollis-Hallett's oscillation experiments.

The experimental helium is contained in a can filled with closely spaced disks (figure 1). This can, initially at rest, is suddenly brought into rotation with a uniform angular velocity ω_0 in the range 0·1 to 1·1 rad/s; as the liquid gradually accelerates a torque must be exerted on the can in order to maintain its uniform motion. The experiment consists in measuring this torque as a function of time, and also the corresponding torque when the can is suddenly brought to rest after the liquid has attained rotational equilibrium; for technical reasons described in § 2 the retardation process has in fact been investigated much more fully than the acceleration process. By integrating the observed torque-time curves the angular momentum of the liquid corresponding to each value of torque during the accelerated motion can be found, so that the time averaging effect of the oscillation experiment is eliminated.

All the measurements have been made at a temperature of 1·27° K, at which the normal fluid density is only 4 % of the total density of the liquid; in these circumstances the normal fluid is tightly coupled to the disk system by its viscosity, and the observed torque can be considered as entirely due to the acceleration of the superfluid. This considerably simplifies the interpretation of the results.

An examination of the qualitative properties of the motion, given in § 3, shows that the frictional forces are dependent on the past history of the liquid, as has been found by Vinen (1957*b*) for the mutual friction in a heat flow. This suggests that the results may be interpreted in terms of a mutual friction due to the presence of vortex lines in the superfluid; such vortex lines may be either the uniform array in the steadily rotating liquid (Feynman 1955; Hall & Vinen 1956*a*, *b*) or an irregular array corresponding to turbulence. A quantitative analysis on this basis is carried out in §§ 4 and 5. In § 4 the equilibrium turbulent intensity appropriate to a steady flow is deduced, and found to be in good agreement with the results of other experiments; in § 5 the growth and decay of turbulence in a non-equilibrium situation is examined. These quantitative considerations reveal two new results that provide further support for the idea of superfluid turbulence; the friction is greatly enhanced by roughening the disk surfaces, and the superfluid flow shows a strong tendency to be macroscopically irrotational.

Preliminary notes of this work have already appeared (Hall & Vinen 1955; Hall 1955).

2. Apparatus

In order to realize the experiment outlined in § 1 the disk-filled can is rigidly attached to the coil of a galvanometer amplifier which can be rotated about its axis of suspension by an electric motor. The feedback amplifier acts as a servomechanism and constrains the can to follow the rotation of the point of suspension within about 10^{-5} rad, and at the same time produces a voltage proportional to the torque exerted on the can in order to maintain this constraint.

(*a*) *The torque-measuring device*

The cryostat, shown schematically in figure 1, is essentially a combination of the constant level cryostat of Atkins (1950) and the demountable torsion head of Hollis-Hallett (1952*b*), in which provision is made for rotation of the torsion head. In figure 1 capital letters have been used to label those parts of the apparatus that are rotated by the electric motor (essentially the casing of the galvanometer), small letters for the fixed part of the cryostat, and greek letters for the suspended system of the galvanometer, which is constrained by feedback to follow the directly driven part.

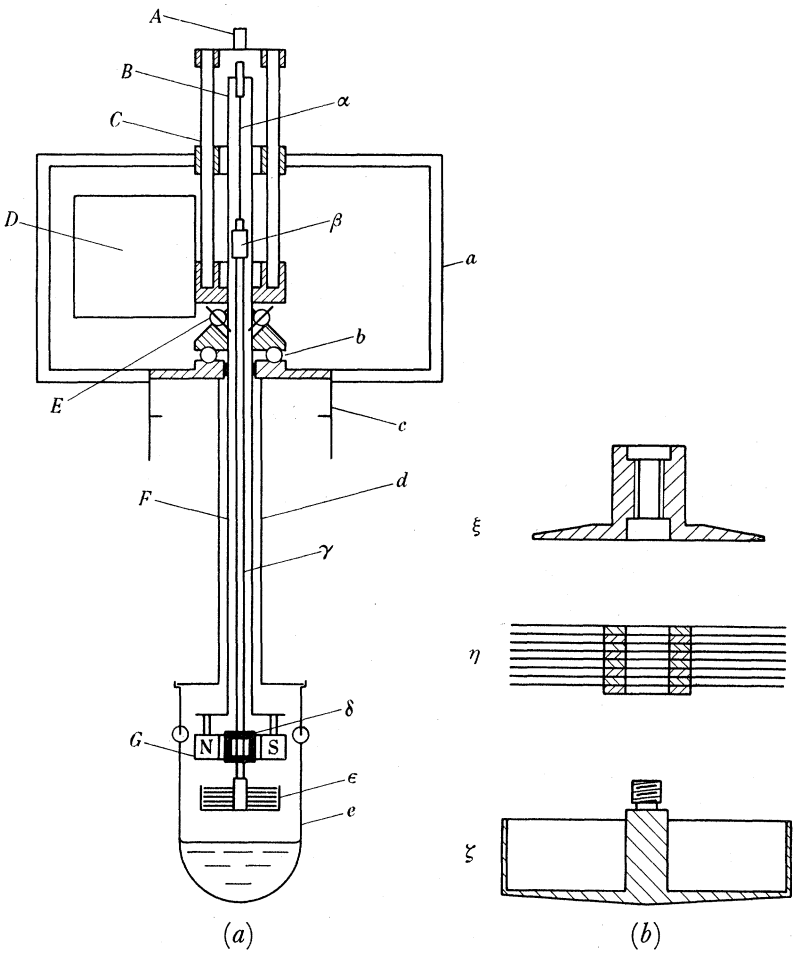

FIGURE 1. (*a*) Schematic drawing of the cryostat; (*b*) a disk-filled can.

The cryostat cap *c* carries a vacuum gland and ball race *b*, and the frame *a*, which together serve to locate the rotating part of the cryostat. The glass vessel *e*, connected to the cryostat cap by the copper-nickel tube *d*, contains a constant amount of liquid helium from which the can ϵ is filled by means of a winch operated bucket (omitted from the figure to avoid confusion; also omitted are the valves used to fill the inner vessel *e* from the outer helium bath). The suspended system of the galvanometer hangs from the torsion head *B* on the 0·002 in. beryllium-copper wire α, and consists essentially of the fused quartz rod γ with a mirror β at the top and the coil δ and disk-filled can ϵ at the bottom. The torsion head *B* continues as the copper nickel tube *F* in order to carry the galvanometer magnet *G*.

Both the torsion head B and the galvanometer optical system D are rigidly attached to the framework C, which can be driven at A by a $\frac{1}{4}$ h.p. three-phase synchronous motor via a reduction gearbox designed to give eight speeds of rotation in the range 0·1 to 1·1 rad/s. The motor accelerates to full speed in about 1/10 s, and can be stopped in a similar time by applying direct current to the windings. The leads to the galvanometer coil δ are brought up the quartz rod γ and connected by springs of 0·0014 in. beryllium-copper to wires passing through the nicoseals E. These leads and those to the optical system D are connected to a system of concentric mercury-filled troughs mounted on the output shaft of the reduction gearbox; contact is made by wires dipping into these troughs.

The optical system D consists of a lamp, two vacuum photocells, and the first valve of the feedback amplifier, mounted on a rigid brass framework. An image of the lamp filament (a straight coil 5×1 mm) is focused via the mirror β onto the junction between two 45° prisms, which reflect the light differentially on to the two photocell cathodes. The lamp filament itself is used as a source, instead of an illuminated aperture, in order to obtain high sensitivity with a beam throw of only 2 cm. The signal from the photocells is amplified by a conventional d.c. amplifier and fed back into the galvanometer coil through a resistance-capacity network designed so that the torque sensitivity of the apparatus can be adjusted by changing the effective resistance, while always retaining the correct amount of phase advance for critical damping. With this arrangement the response time is proportional to the square root of the sensitivity, and is about 1/20 s when full output corresponds to 0·3 dyn cm. The output of the amplifier is connected to the Y plates of an oscilloscope and recorded photographically on moving film. When rotation is started or stopped a considerable impulsive torque is required to accelerate or decelerate the can; this is provided by an auxiliary amplifier, in parallel with the main amplifier and capable of delivering much larger currents without saturating, which is brought into circuit by suitably placed diodes when the main amplifier saturates,

Additional torque can be applied to the suspended system by injecting current into the galvanometer coil from a high impedance source; this method is used both for adjusting the zero of the instrument and for calibration. The principle of the calibration method is to compare the torque signal caused by injecting a definite current with the angular deflexion caused by the same current when feedback is removed; the torque corresponding to this deflexion is deduced from the torsion constant of the suspension fibre, which is determined in the usual way by measuring the period of free oscillations of the suspended system, with and without a known moment of inertia attached.

The whole cryostat is mounted on a flexible support, and driven through flexible couplings, in order to isolate it as far as possible from mechanical vibration.

(*b*) *The can and disk systems*

Figure 1 (*b*) shows the component parts of a typical disk-filled can; in use the disks and spacers η are fixed in the can ζ by screwing down the clamping piece ξ, which in turn screws on to an attachment cemented to the bottom of the quartz rod γ. The clamping piece ξ and the can ζ are turned from solid Duralumin, with the outer parts as thin as possible to keep the moment of inertia low; the purpose of the tapered base to the can is to ensure that helium emerging by film flow drops neatly from the centre of the base. The disks are of

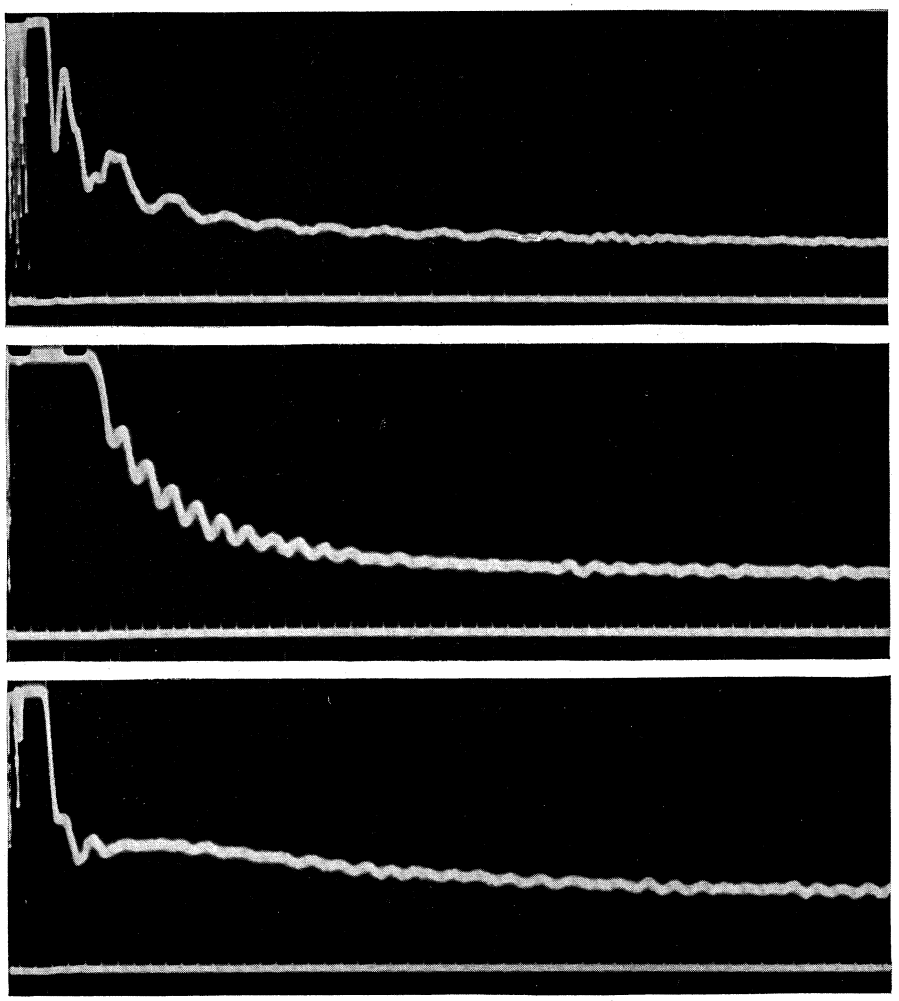

	ω_0	width of film
(*a*)	0·785 rad/s	≈ 0·4 dyn cm
(*b*)	0·785	≈ 0·04
(*c*)	0·196	≈ 0·02

FIGURE 2. Torque-time curves for retardation of the liquid in can OA (upper trace) with timing marks at 1s intervals (lower trace).

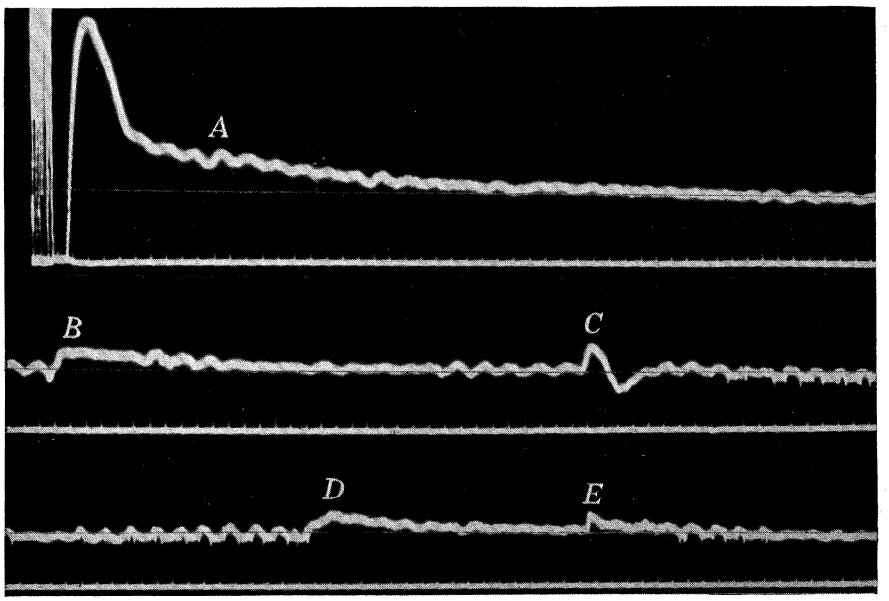

FIGURE 5. The torque pulses observed with can II C during retardation from an initial speed of 0·196 rad/s.

(*Facing p.* 363)

PHILOSOPHICAL TRANSACTIONS OF THE ROYAL SOCIETY A MATHEMATICAL, PHYSICAL & ENGINEERING SCIENCES

mica cleaved to about 0·001 in. thick; they are made by the technique described by Hollis-Hallett (1952*a*), except that each disk is turned individually; this increases the yield of the disk-cutting process to over 90 %. For some disk systems an artificially roughened surface was produced by dipping the disks in a thin paste of grains of Alundum no. 320 and Durofix, draining off the surplus, and allowing the residue to dry. This produced a fairly uniform and closely packed layer of grains on the surface; the grains were of irregular shape with a typical long dimension in the range 0·001 to 0·002 in. Details of the seven disk systems used to obtain the results presented in this paper are given in table 1.

TABLE 1

can	number of disks	diameter of spacers (cm)	disk surface	disk separation (mm)
OA	35	0·95	smooth	0·185
IA	28	2·48	smooth	0·231
IIC	73	2·48	smooth	0·077
IIIC	15	0·95	rough	0·44
IIID	8	0·95	rough	0·91
IIIE	8	0·95	smooth	0·93
IIIF	16	0·95	smooth	0·46

Notes. The inside diameter of the cans was 3·14 cm, the outside diameter of the disks 3·12 cm. The small diameter spacers were of aluminium, the thinnest ones stamped from sheet, the others turned from solid. The large diameter spacers were made of mica in the same way as the disks; they had a mean thickness of 77 μ with an extreme variation of 20 %; they were used singly in can IIC and in groups of three in can IA.

(*c*) *Performance of the apparatus*

The apparatus described above fulfils its servomechanism function satisfactorily at all times, but proves to be capable of measuring torques only when it is stationary, i.e. during retardation of the liquid. During rotation a large irregular oscillatory signal appears on the output of the amplifier, representing the torque required to cause the can to follow the slight irregularities in rotation due to the teeth of the reduction gearing. The only way to make torque measurements during rotation is to filter out this noise by drastically increasing the response time of the instrument. This can be done by dispensing with the feedback system (the copper former on which the coil is wound provides adequate damping), and successful measurements of the final stages of the acceleration process at high speeds have been made in this way (the increased response time precludes measurement of the early stages of acceleration by this method). Further information about the acceleration process can only be deduced indirectly from measurements on retardation, as will be described in § 3 (*c*).

Some typical oscilloscope traces of torque against time during retardation are shown in figure 2 (plate 4). Figures 2 (*a*) and (*b*) show retardation from a high speed at two sensitivities and figure 2 (*c*) shows retardation from a slow speed. The rapid irregular oscillations at the extreme left of the traces are the torque noise during rotation referred to above; this is followed by the impulsive torque required to bring the can to rest, which is provided by the auxiliary amplifier; the main amplifier then regains control and the torque due to retardation of the liquid is observed. Superposed on this signal are oscillations of period about 1 s and $\frac{1}{3}$ s which are due to pendulum type oscillation of the suspended system. These oscillations are excited, and appear as an apparent torque, because of unavoidable inertial asymmetry of the suspended system; they were usually of about the magnitude

shown in figure 2, though occasionally they were smaller; it should be emphasized that in no experiment were they large enough for transverse oscillation of the can to be observed when it was viewed through a cathetometer. The torque required to retard the liquid corresponds to the mean level of these oscillations; it was determined by tracing an enlarged image of the photographic record on a sheet of graph paper and drawing a curve through the centre of the oscillation pattern by eye. This procedure usually gave a reproducibility of about 5 % between repetitions of the experiment; all the results reported here are the mean of at least two readings at each torque sensitivity used. It can be seen from figure 2 (*a*), however, that the oscillations unfortunately prevent any reliable estimate of the torque during the first 2 s of retardation at the highest speed. The torque-time curves obtained in this way were corrected for the response time of the instrument by the approximate, but sufficiently accurate, method of subtracting the response time from the apparent time at which each value of torque occurred (this procedure is exact if the torque-time curve has a constant slope); the response time was deduced from the response to a step function input (the calibration signal).

The correct functioning of the apparatus was checked by making measurements in helium I at a temperature about 0·02° K above the λ-point with the widest disk separation (cans III D and III E). The torque was found to decay exponentially with time, in agreement with the theoretical result given in § 3 (*a*) (equation (2)), and the time constant of decay was found to be independent of initial velocity and surface roughness, as it should be at the low Reynolds numbers used. By fitting equation (2) to the observations values of the density and viscosity can be deduced. The density deduced from the area of the torque-time curves agrees with the directly measured value within the experimental accuracy of about 5 %; this provides a useful check on the torque calibration of the apparatus. Substitution of the observed time constant of decay in equation (2) gives $\eta = 32 \pm 3\,\mu$P; this value is reduced by about 10 % if allowance is made for the extra drag at the edge of the disks due to the wall of the can, and is then in agreement with the value deduced by Donnelly Chester, Walmsley & Lane (1956) from observations on the free surface of accelerating helium. But these viscosities deduced from acceleration experiments are about 20 % higher than those obtained by measurements on capillary flow (Bowers & Mendelssohn 1950); the reason for this discrepancy remains mysterious.

3. Qualitative features of the results

(*a*) *The shape of the retardation curves*

In figure 3 (*a*) the retarding torque is plotted logarithmically as a function of time for a typical disk system at various initial angular velocities. It can be seen that for a high initial angular velocity the torque decays with a steadily increasing time constant during the whole of the observed part of the retardation, but for a low initial angular velocity the torque is nearly constant during the first few seconds of retardation, and only starts to decay later. These general features, which were observed with all disk systems, may also be seen in the photographs of figure 2. In order to understand their significance it is convenient to consider the kinematic consequences of certain simple postulates about the retarding force. If this force is a function only of the relative velocity of superfluid and can, and if the super-

fluid moves as a solid body, the retarding torque G will be a function only of the superfluid angular momentum J; integration of the equation of motion then shows that G is likewise a unique function of the time, apart from an integration constant depending on the initial angular momentum J_0, i.e.

$$G = \phi(t+t_0), \tag{1}$$

where

$$G(t_0) = G(J_0).$$

In general, for a non-linear force, the superfluid will not move as a solid body, but calculation shows that equation (1) will still be valid to a close approximation. If, on the other hand, the retardation mechanism is an ordinary viscosity, solution of the Navier–Stokes equation (cf. Carslaw & Jaeger 1947) shows that the torque is given by

$$G = J_0 \frac{8\nu}{d^2} \sum_{n=0}^{\infty} \exp\left(-\frac{\nu(2n+1)^2\pi^2 t}{d^2}\right), \tag{2}$$

if edge effects are neglected, where ν is the kinematic viscosity and d is the disk separation. Except at the very beginning of the retardation process only the first term of the series makes an appreciable contribution, and if the terms for $n>0$ are ignored, equation (2) is of the form of equation (1), although the function ϕ now depends on disk separation. These two examples suggest that any retardation mechanism depending only on velocities and velocity gradients will give results that obey equation (1) quite closely, although the function ϕ may depend on disk separation in a variety of ways, depending on the precise form of the forces.

But the experimental results certainly do not obey equation (1). The curves of figure 3 (*a*) cannot be made to coincide by displacing them along the time axis, except possibly during the final stages of retardation. This failure of equation (1) suggests that the frictional forces must depend not only on the existing velocities, as assumed above, but also on their past history.

It is also of interest to compare the *shape* of the torque-time curves for different values of the initial angular velocity ω_0. If the superfluid is initially rotating with the can and is eventually brought to rest, curves of G/ω_0 against time should enclose a constant area equal to the moment of inertia I of the superfluid. Similarity of shape can therefore be tested by trying to find a scaling factor $k(\omega_0)$ which will bring the various curves of $k(\omega_0)\, G/\omega_0$ against $t/k(\omega_0)$ into coincidence. This is done in figure 3 (*b*) for the data of figure 3 (*a*), with $k(\omega_0) \propto \omega_0^{-1}$. It can be seen that the curves for high speeds do very nearly coincide, so that the retardation process can be described by a single time constant $k(\omega_0)$. This result is not trivial if, as we have found above, the forces are dependent on past history. For in these circumstances two characteristic times can be defined: J/G the acceleration time constant; and the time constant determining the length of past history this is effective. The implication of figure 3 (*b*) is therefore that at high speeds these two time constants are related by a constant numerical factor; we shall return to this point in § 5 (*b*). Figure 3 (*b*) also shows that the curve for the lowest speed falls entirely below those for high speeds; this implies that less than the total angular momentum is being collected, so that either the superfluid is initially not rotating at the full speed ω_0, or else it is still rotating when no further torque is detectable. In the next section evidence will be presented to show that at least a part of the missing angular momentum is retained in a 'persistent current' of long lifetime. There

is no direct experimental evidence about the completeness of the acceleration process at low speeds, but there are theoretical reasons, supported by experimental evidence (Hall & Vinen 1956*b*) for believing that, if the superfluid is brought into rotation at all, it must rotate very nearly in synchronism with the containing vessel. It will therefore be assumed in what follows that any incomplete collection of angular momentum is entirely due to incomplete retardation.

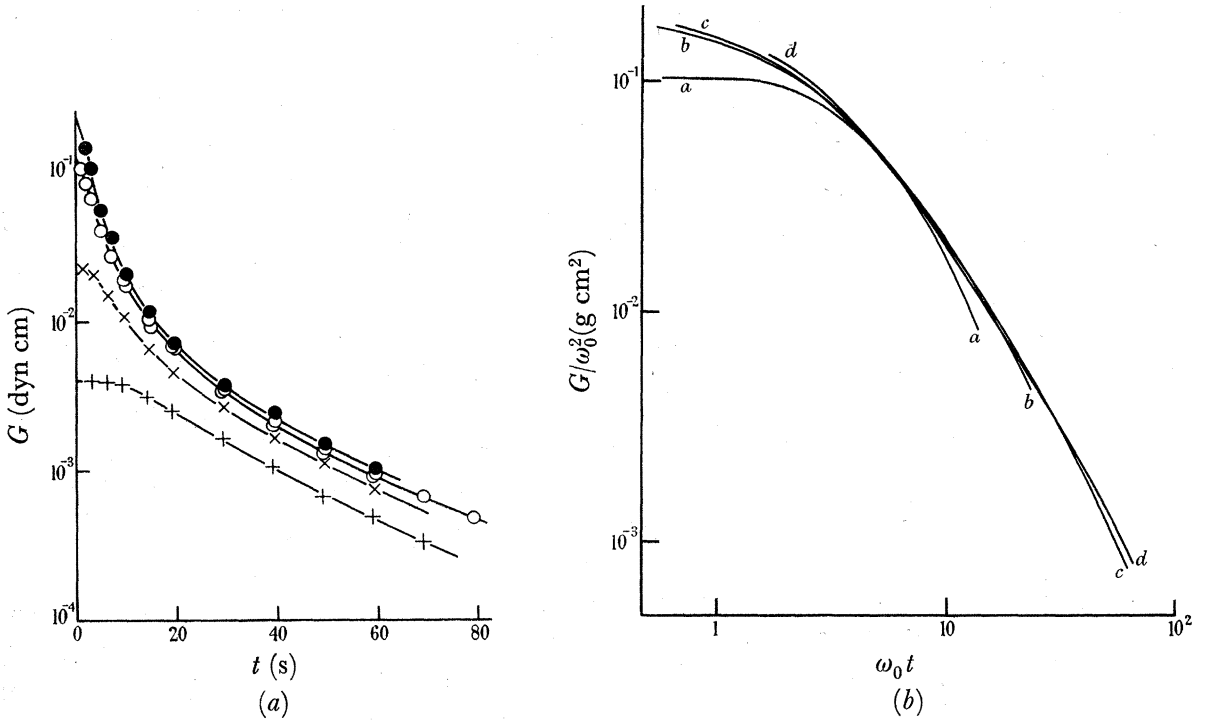

FIGURE 3. Torque-time curves for retardation of the liquid in can IIIF; (*a*) as observed; (*b*) scaled to test similarity of shape. + and curve *a*, $\omega_0 = 0{\cdot}196$ rad/s; × and curve *b*, $\omega_0 = 0{\cdot}393$ rad/s; ○ and curve *c*, $\omega_0 = 0{\cdot}785$ rad/s; ● and curve *d*, $\omega_0 = 1{\cdot}100$ rad/s.

(*b*) *The amount of angular momentum collected*

The amount of angular momentum collected can be obtained by numerical integration of the observed torque-time curves; the principal source of error in the result is the difficulty of extrapolating the observations to $t = 0$ and $t = \infty$. An exponential extrapolation to $t = \infty$ is used; the measurements are continued to sufficiently small torques for any error in this procedure to be negligible except at the lowest speeds. The extrapolation to $t = 0$ is chiefly troublesome at high speeds, where the torque changes rapidly during the first few seconds of retardation; the similarity of curves for different speeds on a graph such as figure 3(*b*) is used as a guide in this extrapolation. These extrapolation difficulties mean that at all speeds the amount of angular momentum collected is uncertain by about 10 % of the solid body value, $I\omega_0$.

The fraction of angular momentum which remains when no further torque is detectable is given by $(1 - J/J_0)$, where J is the angular momentum collected and $J_0 = I\omega_0$; it is plotted against $1/\omega_0$ in figure 4. The figure shows no significant dependence of residual angular momentum on disk separation or surface roughness, but there is a significant increase with increasing spacer diameter. The retention of a greater proportion of angular momentum

when the hole through the centre of the experimental helium is larger suggests at once that we are dealing with an irrotational persistent current, limited by a critical velocity on the inside edge. To test this idea the oblique lines have been drawn on figure 4; they show the expected retention of angular momentum if the critical velocity $v_c = 0{\cdot}2$ cm/s. The horizontal continuations of these lines show the maximum fraction of angular momentum it is possible to retain if the velocity at the inside edge of the persistent current is required not to exceed its initial value. The experimental results do not agree with the drawn lines; the apparent critical velocity is less than 0·2 cm/s for high initial angular velocities, and at low initial angular velocities more angular momentum is retained by the disk systems with small diameter spacers than is possible for the type of persistent current considered here. The reason for these effects will be discussed in § 4.

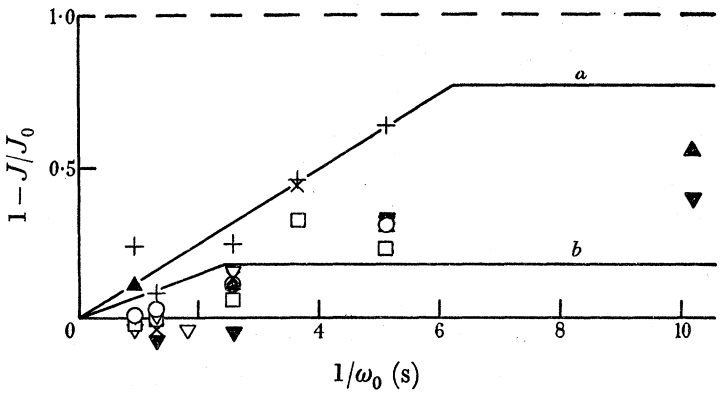

FIGURE 4. The fraction of angular momentum retained as a function of initial angular velocity. +, can IIC; ×, can IA; ▽, can OA; ○, can IIIF; □, can IIIE; ▼, can IIIC; ▲, can IIID. Full lines, expected result for an irrotational persistent current if $v_c = 0{\cdot}2$ cm/s; *a*, for cans with large diameter spacers; *b*, for cans with small diameter spacers.

With the smaller disk separations a curious effect was observed which enabled some information to be obtained about the missing angular momentum; the effect was particularly well marked with can IIC (the smallest disk separation) and was investigated in detail. Figure 5 (plate 4) shows three sections of the torque-time curve observed when this can was stopped after rotation at 0·196 rad/s; the line drawn on the trace indicates the zero of torque, obtained by extrapolating a line drawn through the trace for the interval from 7 to 15 min after stopping. The first section, *A*, is the normal retardation curve, corresponding to the collection of about 30 % of the total angular momentum; after about 2 min the torque pulse beginning at *B* occurs, and is followed by the irregularity *C*; after a further 2 min the pulse *D* occurs, followed shortly by the small pulse *E*. The intervals at which the pulses occur are not completely regular (they vary by several parts per cent in a random way) but the sequence *BCDE* is reproducible, so that a given pulse can be identified. The irregularity *C* does not enclose any net area, and no convincing explanation of its existence has been devised, but the remaining pulses do represent a genuine loss of angular momentum, for they change sign when the direction of rotation is changed so that they are always in the same sense as the main part of the retardation curve. This direct association between the pulses and the residual angular momentum is confirmed by the observation that the pulses

observed after a higher initial speed of rotation are smaller; within the experimental accuracy the reduction in pulse size agrees with the reduction in residual angular momentum deduced from the areas of the torque-time curves. The pulse size can therefore be regarded as a measure of the residual angular momentum; the mere fact that pulses occur 4 min after rotation is stopped shows that the superfluid is still rotating at that time.

The pulses appear to be associated with the emptying of the can by film flow, for none are observed if the liquid level in the inner chamber (*e* in figure 1) is arranged to be only just below the rim of the can. It is most unlikely that this modification has any effect other than the prevention of film flow, since the only contact between liquid inside and outside the can is via vapour and the film. A *continuous* torque due to emptying by film flow is to be expected, if the film does not carry away angular momentum, due to the term $\omega \mathrm{d}I/\mathrm{d}t$ in $\mathrm{d}(I\omega)/\mathrm{d}t$, but this effect is unobservedly small. A possible explanation of the observed discontinuous loss of angular momentum is as follows. As the can empties, surface tension may retain liquid for a time between a pair of disks above the liquid level at the rim of the can, but this arrangement is not stable and at some stage the annulus of liquid will split and drain out; as soon as the annulus splits, and thus becomes simply connected, an irrotational persistent current is no longer possible and the angular momentum will be collected. One defect of this tentative explanation is that the observed size and spacing of the pulses (each of the groups *BC*, *DE* corresponds to the residual angular momentum between about ten disks) seems to require that the break-up should occur between several disks at once; however, no more satisfactory explanation has been devised. It should be emphasized that the arguments of this section in no way depend on these speculations concerning the mechanism by which the pulses appear; they depend only on the experimental fact of a spontaneous loss of angular momentum controlled by film flow.

This fact suggests a method of controlling the time at which the pulses appear, and hence of comparing the residual angular momentum at different times after the stopping of the can. If the can is surrounded by a second vessel filled with liquid helium so that initially the common liquid level is just below the rim of the can, film flow will at first occur only from the outer vessel, the liquid being retained in the can by surface tension; film flow from the can will not start until the level in the outer vessel has fallen by an amount equal to the surface tension rise for the gaps in the can. The filling bucket, used to fill the can from the inner helium bath, can be used as an auxiliary vessel in this way, with the result that the onset of film flow from the can is delayed by about 10 min. By comparing the areas under the pulse *D* with normal and delayed film flow it was found that the residual angular momentum decayed by 15 ± 30 % in the interval from 4 to 14 min after the can was stopped. The lifetime of the persistent current is therefore greater than 25 min, and may possibly be infinite. This may be compared with the lifetime of about 1/30 s for a current of helium 1 in the same disk system.

(*c*) *Comparison of the acceleration and retardation processes*

So far only the process of retardation from a state of equilibrium with a uniformly rotating vessel has been considered. It is important to know whether the acceleration process is equivalent in order to decide whether absolute angular velocity is an important parameter in the equations of motion. This matter has been investigated fairly thoroughly

with can OA at a speed of 0·785 rad/s. As was explained in § 2 (*c*), it is only possible to investigate the final stages of the acceleration process directly. The indirect method used to investigate the greater part of the process depends on the fact that at the comparatively high speed of rotation used there is no significant retention of angular momentum on retardation. Therefore, if the can is stopped after rotation for a time t the angular momentum collected is equal to the angular momentum imparted to the liquid, initially at rest, in time t; by varying t the fraction of the full angular momentum taken up can be found as a function of time. The results are shown in figure 6 (*a*), together with results obtained by

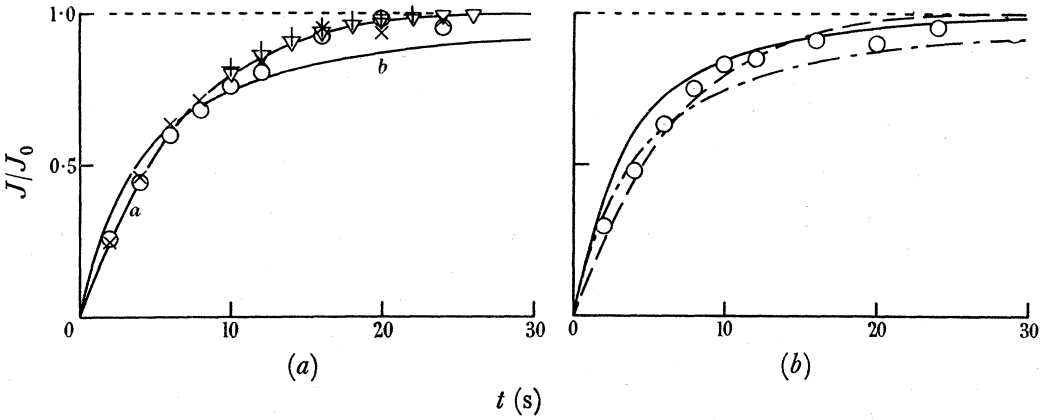

FIGURE 6. The superfluid angular momentum as a function of time during acceleration and retardation; $\omega_0 = 0{\cdot}785$ rad/s. (*a*) can OA: ○ and ×, acceleration measurements by the indirect method, made 5 and 1 min, respectively, after the previous rotation; ▽ and +, acceleration measurements by the direct method, made 1 and < 1 min, respectively, after the previous rotation; *a*, mean acceleration curve; *b*, mean retardation curve. (*b*) can IA: ○, acceleration measurements by the indirect method, made 1 min after the previous rotation; ——, mean retardation curve; ———, mean acceleration curve for can OA; —·—·—, mean retardation curve for can OA.

the direct method, which is much more accurate when it can be used, i.e. during the final stages of acceleration; also shown is the corresponding curve for the fraction of angular momentum lost as a function of time during retardation. It is quite clear that the two processes are not equivalent; acceleration begins more slowly and finishes more rapidly than retardation. In other words, for a given relative angular velocity of can and superfluid the frictional forces are greater if the absolute angular velocity of the superfluid is greater. Measurements on can IA by the indirect method, shown in figure 6 (*b*), give qualitatively similar results. This can has a similar disk separation to can OA, but large diameter spacers between the disks; the reason for the quantitative differences will be discussed in § 4.

These results are of the form to be expected if the frictional forces include a mutual friction $B(\rho_s\rho_n/\rho)\,\omega(v_s - v_n)$ per unit volume, as deduced from the attenuation of second sound in helium rotating uniformly with angular velocity ω (Hall & Vinen 1956*a*), provided that ω is interpreted as the angular velocity of the superfluid, in accordance with theoretical expectation. If it is supposed that the remaining friction is the same for both acceleration and retardation the initial slopes of the acceleration and retardation curves in figure 6

should differ by $B(\rho_n/\rho)\,\omega_0$ (compare next section); the measured slopes give $B = 1{\cdot}6 \pm 0{\cdot}5$,* in good agreement with the second sound results. This agreement is, however, probably somewhat fortuitous, for the more detailed considerations of §§ 4 and 5 will show that other effects contribute to the asymmetry between acceleration and retardation.

It may be mentioned that acceleration measurements were also made for various intervals between the start of the measured rotation and the stopping of the previous rotation. The idea behind this experiment was that if the time-dependent friction due to the previous rotation did not decay completely the observed acceleration might be more rapid. It can be seen from figure 6(*a*) that the differences between the various sets of points are in the sense expected from this idea, but are hardly large enough to be significant.

4. The equilibrium frictional forces

We have seen above that the observed frictional forces probably include the mutual friction $B(\rho_s\rho_n/\rho)\,\omega(v_s - v_n)$, at any rate at the beginning of retardation, and that the remaining friction is dependent on the past history of the liquid with a time scale of the order of the acceleration time scale. Such a long time scale in a liquid suggests that the phenomenon is connected with turbulence; when we recall that the mutual friction in uniformly rotating helium can be accounted for by the presence of vortex lines in the rotating liquid (Hall & Vinen 1956*b*), it seems reasonable to suppose that a turbulent array of vortex lines will likewise give rise to mutual friction. Independent evidence for the idea that turbulence gives rise to mutual friction is provided by the observation of transient attenuations of second sound during angular acceleration (Hall & Vinen 1956*a*) and by experiments on heat flow (Vinen 1957*a*, *b*). We shall therefore make the hypothesis that the observed friction can be completely described by a mutual friction due to the presence of vortex lines; the observed forces on the superfluid will accordingly be written as $F_{sn} = B(\rho_s\rho_n/\rho)\,\Omega(v_s - v_n)$ per unit volume, thereby defining a quantity Ω which is expected to be proportional to the total length of vortex line in unit volume. The remainder of this paper will be devoted to a detailed quantitative examination of the behaviour of the quantity Ω, in order to see whether it behaves as might be expected for an intensity of turbulence; the experimental data for this purpose are the torque-time curves observed during retardation.

If the disk separation is sufficiently small for the normal fluid to be effectively held at rest by its viscosity and if the superfluid is retarded solely by the force $B(\rho_s\rho_n/\rho)\,\omega(v_s - v_n)$ it is easily shown that the torque G is given by

$$\frac{G}{I\omega} = B\frac{\rho_n}{\rho}\omega, \tag{3}$$

where I is the moment of inertia of the superfluid considered as a solid body (it moves as a solid body for this essentially linear force). By analogy with equation (3) we can write in the general case

$$\frac{G}{I\bar{\omega}} = B\frac{\rho_n}{\rho}\bar{\Omega}, \tag{4}$$

* The upper limit $B = 6{\cdot}3 \pm 0{\cdot}5$ estimated from preliminary results (Hall 1955; Hall & Vinen 1955) was obtained from retardation measurements on the assumption that the remaining friction obeyed a Gorter–Mellink law with a value of $34\,\mathrm{P}^{-1}$ for the constant A, chosen to give the best fit to capillary flow measurements (Atkins 1951). It will be seen in §4 that this assumption was incorrect.

where the average angular velocity $\bar{\omega} = J/I$, and $\bar{\Omega}$ is a suitable average of Ω defined by equation (4). The value of $\bar{\omega}$ for each value of G during the retardation process can be found by numerical integration of the torque-time curves, as explained in § 3 (*b*), and hence $G/I\bar{\omega}$ can be found as a function of $\bar{\omega}$; results for a typical disk system are shown in figure 7. The curves show very clearly that the frictional force is not a unique function of angular velocity; for any given value of $\bar{\omega}$ several intensities of turbulence can exist, depending on the previous history of the helium. It can now be seen that the decrease in residual angular momentum with increasing initial angular velocity, which was noted in § 3 (*b*), is due to the time dependence of the turbulence. For a larger initial angular velocity a stronger turbulence is generated; this takes longer to decay, and consequently the superfluid loses more angular momentum before retardation finally ceases; this accounts for the failure of earlier attempts (Osborne, private communication; Andronikashvili 1952) to observe a

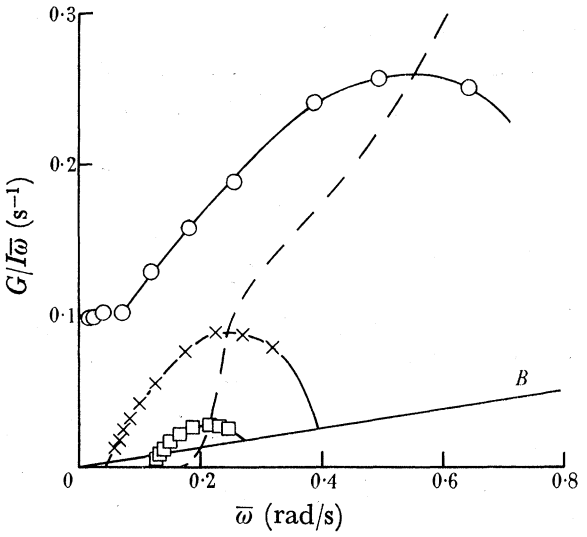

FIGURE 7. The variation of turbulent intensity with angular velocity during retardation for can IA. □, $\omega_0 = 0{\cdot}275$ rad/s; ×, $\omega_0 = 0{\cdot}393$ rad/s; ○, $\omega_0 = 0{\cdot}785$ rad/s; ———, the equilibrium turbulent intensity. The line *B* represents equation (3).

persistent current. The straight line *B* in figure 7 represents equation (3); if no turbulence is initially present $G/I\bar{\omega}$ will start from a point on this line. It might be thought that the amount of vortex line due to uniform rotation, represented by the line *B*, should be subtracted from $G/I\bar{\omega}$ to obtain the intensity of turbulence; we shall, however, regard the whole of the vortex line present during the observed part of the retardation as turbulence, for reasons that will become apparent in § 4 (*a*). The variation of $G/I\bar{\omega}$ with time can be seen by following the curves of figure 7 from right to left; the turbulence at first grows and then decays, so that each curve is characterized by a maximum in $\bar{\Omega}$ at a fairly early stage in the retardation. Thus, in the $(\bar{\Omega}, \bar{\omega})$ plane (effectively this is what is shown in the figure) there is a locus on which $\mathrm{d}\bar{\Omega}/\mathrm{d}t = 0$ (broken curve in figure 7); to the left of this locus $\mathrm{d}\bar{\Omega}/\mathrm{d}t$ is negative and to the right it is positive. In other words the locus of the maxima of the observed $\bar{\Omega}(\bar{\omega})$ curves represents a stable intensity which the turbulence is always trying to approach. It will be supposed that this stable turbulent intensity is, for any given value of $\bar{\omega}$, the equilibrium intensity that the turbulence would assume if that value of $\bar{\omega}$

were somehow maintained indefinitely. This assumption, though plausible, is not quite obvious; it amounts, in fact, to assuming that

$$d\bar{\Omega}/dt = \phi(\bar{\Omega}, \bar{\omega}), \tag{5}$$

i.e. that the rate of growth or decay of the turbulence is controlled only by the existing turbulent intensity and fluid velocities (and not, for example, by the acceleration of the liquid), and also that the operation of averaging over the experimental helium does not appreciably affect this functional relation. In one or two cases the experimental results appear to contradict equation (5), by the intersection of two $\bar{\Omega}(\bar{\omega})$ curves, indicating two values of $d\Omega/dt$ at a single point in the $(\bar{\Omega}, \bar{\omega})$ plane. This anomaly, however, is almost certainly due to systematic error in the values of $\bar{\omega}$ for a single retardation process, due to the extrapolation difficulties explained in § 3 (*b*). If the uncertainty in the experimental values of $\bar{\omega}$ is borne in mind, there is no experimental reason for doubting equation (5), and its validity will therefore be assumed in what follows.

The equilibrium values of $\bar{\Omega}$, given by the broken curve in figure 7, will be discussed in this section, and the form of the function ϕ will be examined in § 5.

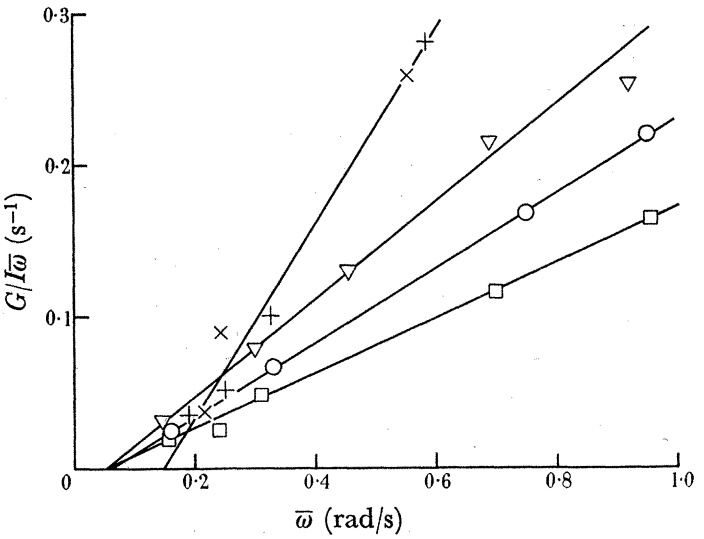

FIGURE 8. The equilibrium turbulent intensity (uncorrected, equation (4)). +, can IIC; ×, can IA; ▽, can OA; ○, can IIIF; □, can IIIE.

(*a*) *The effect of disk separation and spacer diameter*

The equilibrium values of $G/I\bar{\omega}$ for all the systems of smooth disks are shown in figure 8. It can be seen that $G/I\bar{\omega}$ is smaller for the larger disk separations, and varies more rapidly with mean angular velocity for the disk systems with large diameter spacers. These data, however, do not give strictly comparable values for the turbulent intensity in the various disk systems for two reasons. First, a correction must be applied to allow for the fact that at large disk separations and high velocities the normal fluid cannot be considered as held at rest by its viscosity; and secondly the radial averaging implied in $\bar{\Omega}$ is different for disk systems with large and small diameter spacers, so that the results must be suitably scaled to allow for this.

If the normal fluid is not at rest, equation (4) must be replaced by

$$\frac{G}{I\bar{\omega}_r} = B\frac{\rho_n}{\rho}\bar{\Omega}, \tag{6}$$

where $\bar{\omega}_r$ is the mean relative angular velocity of the two fluids. To calculate $\bar{\omega}_r$ we shall assume that Ω and v_s are uniform across the gap between a pair of disks,* and we shall neglect normal fluid inertia since $\rho_n/\rho \ll 1$; the equations of motion then become

$$\eta_n \frac{\mathrm{d}^2 v_r}{\mathrm{d}x^2} = F_{sn} = B\frac{\rho_s \rho_n}{\rho}\Omega v_r, \tag{7}$$

with the boundary condition $v_r = v_s$ at $x = \pm l$, where $v_r = (v_s - v_n)$ and $2l$ is the disk separation. Hence, the average relative velocity between a pair of disks is

$$\bar{v}_r = v_s \frac{\tanh z}{z}, \tag{8}$$

where

$$z = \left(\frac{F_{sn}}{\eta_n \bar{v}_r}\right)^{\frac{1}{2}} l = \left(\frac{B\rho_s \rho_n \Omega}{\rho \eta_n}\right)^{\frac{1}{2}} l. \tag{9}$$

To a first order this can be written in terms of the observed force F_{sn} per unit volume of liquid as

$$\bar{v}_r = v_s - \frac{F_{sn} l^2}{3\eta_n}. \tag{10}$$

Equation (9) is readily integrated over the volume of the liquid between the disks to give the angular momentum of the superfluid relative to the normal fluid as

$$\begin{aligned} J_r = I\bar{\omega}_r &= \int_a^b \rho_s \left(v_s - \frac{F_{sn} l^2}{3\eta_n}\right) 2\pi r^2 h \,\mathrm{d}r \\ &= I\bar{\omega} - \frac{\rho_s l^2}{3\eta_n} G, \end{aligned} \tag{11}$$

where b = inside radius of can,

a = outside radius of spacers,

and h = total height of helium.

Equation (11) shows that to a first order the correction for finite disk separation is independent of the radial variation of superfluid velocity, so that to this approximation the form of the radial averaging can be considered separately. The higher order corrections are somewhat dependent on the radial velocity variation, but we shall for simplicity ignore this effect and take

$$\bar{\omega}_r = \bar{\omega} \tanh\left(\frac{G\rho_s}{I\bar{\omega}_r \eta_n}\right)^{\frac{1}{2}} l \Big/ \left(\frac{G\rho_s}{I\bar{\omega}_r \eta_n}\right)^{\frac{1}{2}} l, \tag{12}$$

which, by equation (8), is the accurate result if the velocities are independent of radius; it should be sufficiently exact when the first order correction is dominant (i.e. when $Gl^2\rho_s/I\bar{\omega}\eta_n < 1$). Values of $\bar{\omega}_r$ can be found by solving equation (12) graphically, and substituted into equation (6) to give $\bar{\Omega}$.

* This assumption does not greatly affect the result; if the superfluid has no rigidity, so that $(v_s - v_n)$ is uniform, the correction is slightly larger.

In order to obtain $\Omega(\bar{v}_r)$ from $\overline{\Omega}(\bar{\omega}_r)$ it is necessary to invert the radial averaging. To do this we assume that $\Omega \propto \bar{v}_r^n$ and $\bar{v}_r \propto r^m$ with sufficient accuracy for the purpose of calculating scaling factors, and take $n = 2$ to give the best overall fit to the data of figure 8. It is then assumed that $\Omega(\bar{v}_r)$ is independent of spacer diameter and m is chosen to make the data for cans OA and IA, which differ appreciably only in spacer diameter, coincide as nearly as possible; the best fit is for $m = -1$.* With $n = 2$ and $m = -1$ we find

$$\overline{\Omega}(\bar{\omega}_r) = \Omega(v_a) \frac{2a^2}{b^2 - a^2} \ln \frac{b}{a}, \tag{13}$$

and

$$v_a = \left(\frac{b^2 + a^2}{2a}\right) \bar{\omega}_r, \tag{14}$$

where v_a is the value of $\bar{v}_r$ at $r = a$ (i.e. the maximum value). Equations (13) and (14) give $\Omega(v_a)$ in terms of $\overline{\Omega}(\bar{\omega}_r)$.

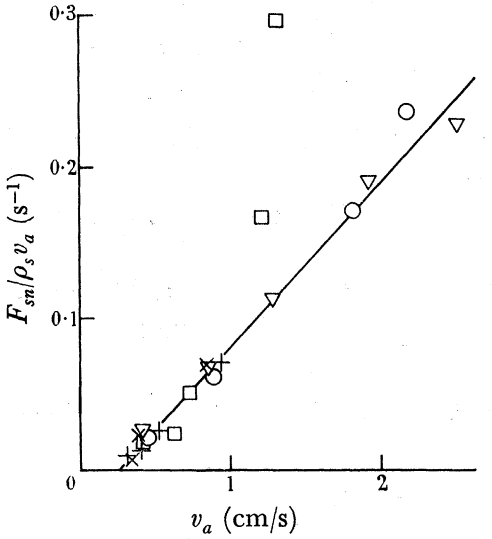

FIGURE 9. The equilibrium turbulent intensity, corrected for the effects of finite disk separation and radial averaging. +, can IIC; ×, can IA; ▽, can OA; ○, can IIIF; □, can IIIE.

The values of $(F_{sn}/\rho_s v_a) = B(\rho_n/\rho)\,\Omega(v_a)$ as a function of v_a deduced from the data of figure 8 are shown in figure 9. It can be seen that the points for all disk systems now fall on a single curve within the experimental error, except for the two highest speeds at the largest disk separation; for these two points $(Gl^2\rho_s/I\bar{\omega}\eta_n) > 1$, and we have already seen that under these conditions the approximate correction procedure used here becomes invalid. It is, therefore, reasonable to ignore these two points and conclude that the equilibrium turbulent intensity is independent of disk separation within the experimental error; this suggests that the equilibrium turbulent intensity depends only on $\bar{v}_r$, and thus provides some *a posteriori* justification for our assumption that it was independent of spacer diameter. It is, of course, impossible to be certain that the interpretation suggested here is unique; but we have at least shown that the results are consistent with the simple assumption of an

* A physically more reasonable assumption would be $v_s \propto r^{-1}$, but this differs appreciably from the simpler assumption $\bar{v}_r \propto r^{-1}$ only when the correction for finite disk separation is so large that equation (12) is probably not valid anyway.

equilibrium turbulent intensity that depends only on relative velocity. Figure 9 suggests that the mutual friction becomes very small at a critical velocity $v_c = 0{\cdot}24 \pm 0{\cdot}05$ cm/s independent of disk separation.

The agreement of the points for large and small diameter spacers is fairly sensitive to the value assumed for m; it is probably safe to conclude that $m = -1 \pm 0{\cdot}2$, i.e. that the flow of the superfluid is very nearly macroscopically irrotational at the instant of maximum turbulence. We saw in § 3 (*b*) that the residual angular momentum was probably irrotational, so it is likely that the flow is irrotational for the whole of the retardation process after the instant of maximum turbulence; it is for this reason that we have regarded the whole of the observed friction as due to turbulence, for the regular array of vortex lines which is present in uniform rotation cannot exist in an irrotational circulation, since curl $\bar{v}_s = 0$.

The rather remarkable conclusion that the superfluid flow is macroscopically irrotational requires some discussion. The state of the superfluid in equilibrium with a rotating vessel is expected to approximate very closely to solid-body rotation because of the possibility of vortex lines (Feynman 1955). But even if it is supposed that, for some unknown reason, the state with vortex lines cannot be formed in our disk systems, so that the equilibrium state is an irrotational circulation, minimization of the free energy (cf. Hall & Vinen 1956*b*) shows that the equilibrium angular momentum would be less than the solid-body value by a factor $(b^2-a^2)/(b^2+a^2)\ln(b/a)$; this factor is 0·695 for the small diameter spacers. Such a ratio of observed to solid-body angular momentum is quite inconsistent with our observations of this quantity at high speeds (§ 3 (*b*)); indeed, the experimental observation that the equilibrium angular momentum is close to the solid-body value implies that the superfluid is rotating very nearly as a solid body with the containing vessel. It must therefore be concluded that the superfluid flow is not at first irrotational, but very rapidly becomes so. This process requires energy, since the kinetic energy for an irrotational circulation is larger than for solid-body rotation with the same angular momentum; calculation shows that the angular momentum must decrease to a fraction $\{(b^2-a^2)/(b^2+a^2)\ln(b/a)\}^{\frac{1}{2}}$ of its initial value before irrotational flow is energetically possible. In fact, rather more angular momentum must be lost in order to provide the turbulent energy, but this is probably only a small percentage of the total kinetic energy, unless many vortex lines of the same sign are grouped together to form large eddies. This energy condition is easily satisfied for the disk systems with large diameter spacers, but for the disk systems with small diameter spacers it is only just satisfied at low velocities, and for some of the points at high velocities irrotational flow is not quite energetically possible at the estimated position of equilibrium turbulence; for this reason the points on figure 9 for $v_a > 1{\cdot}5$ cm/s should be treated with some reserve. From these considerations it seems likely that with small spacers a dominant factor in the initial growth of turbulence is the availability of energy.

It is now necessary to enquire why the superfluid flow becomes irrotational. If the different annular regions are accelerated independently a linear force preserves solid body rotation ($m = +1$) during retardation, and a force that varies more rapidly with velocity tends asymptotically to produce a velocity independent of radius ($m = 0$). There must, therefore, be a force acting between the different annular regions in order to produce an irrotational mean flow; such a force is provided by turbulence, which tends to produce irrotational mean flow by radial mixing with conservation of angular momentum (see, for

PHILOSOPHICAL TRANSACTIONS OF THE ROYAL SOCIETY A MATHEMATICAL, PHYSICAL & ENGINEERING SCIENCES

example, Townsend 1956). In an ordinary liquid this tendency is strongly opposed by the viscous boundary layer, but in superfluid helium the boundary layer no longer exists and the only opposition comes from the tendency of mutual friction to produce a state with $m = 0$. The mean flow of the superfluid is probably more correctly described by an eddy viscosity η_s with the boundary condition $\operatorname{curl} \bar{\mathbf{v}}_s = 0$, but in the present experiments η_s appears to be sufficiently large to ensure that $\operatorname{curl} \bar{\mathbf{v}}_s \doteqdot 0$ everywhere; a rough calculation shows that $\eta_s \gtrsim 10^{-3}$ P.

The transition from uniform rotation to irrotational flow at an early stage of the retardation process implies an acceleration of the inner layers of liquid at the expense of the outer layers, so that the velocity at the inside edge of the helium annulus can exceed the initial value. This accounts for the large residual angular momenta observed with small diameter spacers at low initial angular velocities (§ 3 (*b*)).

Finally, a comment on the differences between the acceleration and retardation processes, shown in figure 6, for cans OA and IA, which differ appreciably only in spacer diameter. The retardation process is much more rapid for can IA, and this difference, as we have seen, is due to the irrotational mean flow of the superfluid. The arguments given above would lead us to expect an irrotational superfluid flow during acceleration also, which would give $m = +1$ at the beginning of acceleration and $m > 1$ later; equations analogous to equation (13) show that this gives a much smaller difference between the two disk systems for the early part of the acceleration process, as is observed. Quantitative comparison of the acceleration and retardation processes for can IA will be given in § 5 (*b*).

(*b*) *Comparison with other experiments*

The data of figure 9 on equilibrium turbulent intensity as a function of relative velocity are replotted in figure 10 in such a way as to give a straight line through the origin for a Gorter–Mellink (1949) law $F_{sn} = A\rho_s\rho_n\bar{v}_r^3$, together with values derived from the mutual friction deduced by Atkins (1951) from measurements on isothermal flow through a 0·0815 mm diameter capillary; these measurements were actually made at 1·22° K, but the experiments showed little variation in the mutual friction at low velocities between 1·22 and 1·52° K. Values of turbulent intensity deduced from experiments with a rotating cylinder viscometer* (Hollis-Hallett 1953; Heikkila & Hollis-Hallett 1955) are also shown in figure 10. As Hollis-Hallett points out, a mutual friction alone should not give rise to any extra torque in this experiment; but if we make the assumptions used in analyzing the present results (rigid superfluid, $\operatorname{curl} \bar{\mathbf{v}}_s = 0$, and equilibrium turbulent intensity controlled by the mean relative velocity), the solution of equation (7) for a plane Couette flow (which is sufficiently close to the flow examined by Hollis-Hallett) can be shown to be

$$\frac{\eta_n + \eta'}{\eta_n} = \frac{z}{\tanh z}, \tag{15}$$

$$\bar{v}_r = \frac{v_1}{z \sinh z}(\cosh z - 1), \tag{16}$$

* *Note added in proof*, 17 *October* 1957. Hollis-Hallett (Fifth international conference on low-temperature physics, Madison, Wisconsin, 1957) has now found similar effects with ordinary liquids in his viscometer. This discovery casts considerable doubt on the interpretation suggested here for his helium II results; it remains possible that the mechanism considered here contributes to the observed torque, but even so the values of turbulent intensity deduced from the viscometer results are probably wrong.

PHILOSOPHICAL TRANSACTIONS OF THE ROYAL SOCIETY A MATHEMATICAL, PHYSICAL & ENGINEERING SCIENCES

where

$$z = \left(\frac{F_{sn}}{\eta_n \bar{v}_r}\right)^{\frac{1}{2}} l = \left(\frac{B\rho_s \rho_n \Omega}{\rho \eta_n}\right)^{\frac{1}{2}} l, \tag{9}$$

η' is the apparent extra viscosity, and the flow is between planes at $x = \pm l$ moving with velocities $\pm v_1$. The points plotted in figure 10 were deduced from the experimental apparent viscosities at 1·27° K with the aid of equations (9), (15) and (16).

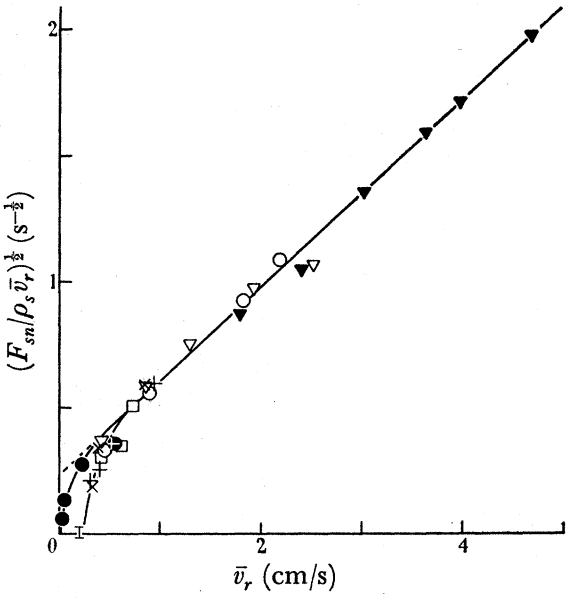

FIGURE 10. The equilibrium mutual friction deduced from isothermal flow experiments at 1·27° K. + × ▽ ○ □, present experiments, as in figure 9; I, estimated from lifetime of persistent current in can IIC; ▼, from capillary-flow experiments (Atkins 1951); ●, from the rotating cylinder viscometer (Hollis-Hallett 1953).

It can be seen that the angular acceleration and capillary flow results are well represented by a modified Gorter–Mellink law

$$F_{sn} = A\rho_s \rho_n (\bar{v}_r - v_0)^2 \bar{v}_r, \tag{17}$$

with

$$A = 23 \pm 2\,\mathrm{P}^{-1},$$

$$v_0 = -0{\cdot}6 \pm 0{\cdot}2\,\mathrm{cm/s},$$

together with a rapid drop in mutual friction below the value given by equation (17) in the vicinity of a critical velocity; this agreement is not remarkable, since the two experiments are very similar. Figure 10 shows that the viscometer results can also be interpreted in this way, with a smaller value of the critical velocity; but they do not extend to sufficiently high velocities for a test of equation (17) to be possible, so that the interpretation suggested here is only tentative, and is certainly not unique; an equally good fit can, for example, be obtained on the assumption that the turbulent intensity is controlled by the *maximum* relative velocity, if the superfluid eddy viscosity η_s is taken as about 30 μP. The value of A required to fit these isothermal flow experiments does not differ significantly from the value of 26·5 P^{-1} obtained by a small extrapolation of Vinen's (1957*a*) results on heat flow to 1·27° K, but the value of v_0 is of the opposite sign to that found by Vinen, though of a similar order of magnitude. It thus appears possible that the differences in equilibrium mutual friction in isothermal and heat flow experiments can be described wholly by the parameter

v_0; the temperature dependence of the capillary flow and viscometer results suggests that the algebraic value of v_0 for isothermal flow increases with increasing temperature, eventually becoming positive, as in a heat flow.

Figure 10 shows that the critical velocity for the viscometer is much smaller than in the present experiments. Examination of the points for the various disk systems shows that only the disk systems with large diameter spacers give any real indication of a critical velocity; the intercept on the velocity axis of figure 9 should therefore not be interpreted as a true critical velocity independent of disk separation. For can II C the measured lifetime of a persistent current (§ 3 (*b*)) shows that the turbulent intensity must decrease by a factor of at least 200 between 0·5 and 0·2 cm/s, and the points for can I A suggest similar behaviour; the question of whether the turbulent intensity really decreases to zero will be discussed in § 5 (*b*).

Hollis-Hallett's (1952*a*) experiments with oscillating disk systems are very similar to the present experiments, and it is therefore probable that they can also be explained in terms of a mutual friction due to turbulence; his conclusion that the results with a single disk and a pile of disks cannot both be explained by a mutual friction will be modified by the existence of a superfluid eddy viscosity and by the time dependence of the turbulence. These experiments, and experiments on the oscillations of helium in a U-tube (Donnelly & Penrose 1956), show a tendency for the helium to behave as a single fluid at high velocities; such behaviour is to be expected at high turbulent intensities, if there are no temperature gradients to make v_s and v_n unequal; the observed increase in viscosity in these circumstances is presumably due to the eddy viscosity of the superfluid. This single-fluid behaviour is also found in angular acceleration experiments at velocities much larger than those used here (Donnelly *et al.* 1956).

(*c*) *The effect of surface roughness*

Measurements at the two largest disk separations with artificially roughened surfaces (§ 2 (*b*)) show that the time scale of the motion is greatly shortened. This has the unfortunate consequence that the experimental accuracy is greatly reduced, and detailed results will therefore not be given; it can, however, be stated that, if the results are treated as in § 4 (*a*), the frictional forces are found to be increased by a factor of about 7 for the larger disk separation (~ 1 mm), and by a factor of about 18 for the smaller separation ($\sim \frac{1}{2}$ mm). These results should be contrasted with Vinen's (1957*a*) finding that surface roughness does not change the mutual friction in a heat flow by more than 1 %. This contrast at once suggests that an important factor is the value of v_s at the boundary, which is smaller relative to $(v_s - v_n)$ by a factor ρ_n/ρ in a heat flow if the superfluid flow is macroscopically irrotational. The rapid dependence of frictional force on disk separation suggests that the acceleration mechanism is essentially a surface drag on the superfluid, which is stiffened by an eddy viscosity; such an effect could arise either from mutual friction in a boundary layer near the wall or from the tension in vortex lines that become attached to surface protuberances.

This marked effect of surface roughness suggests that even the measurements with smooth disks may be affected by surface conditions. Since, however, the equilibrium turbulent intensity is found to be independent of disk separation with smooth disks, it is probable that surface effects are in fact absent.

5. The time dependence of the frictional forces

The equilibrium turbulent intensity $\bar{\Omega}_{eq.}$ was evaluated in § 4 by making the very plausible assumption that the time dependence of the turbulence was governed by an equation of the form

$$d\bar{\Omega}/dt = \phi(\bar{\Omega}, \bar{\omega}). \tag{5}$$

This section will be devoted to an examination of the form of the function ϕ; only the results for the two disk systems with large diameter spacers (cans I A and II C) will be considered, since for these disk systems the complicating effects of finite disk separation and radial averaging are largely absent, and can, for the present purpose, be ignored. We then have

$$\frac{G}{I\bar{\omega}} = B\frac{\rho_n}{\rho}\bar{\Omega}, \tag{4}$$

so that by replotting curves such as those of figure 7 with time as abscissa $d\bar{\Omega}/dt$ can be found for all those points in the $(\bar{\Omega}, \bar{\omega})$ plane which are covered by the experimental results.

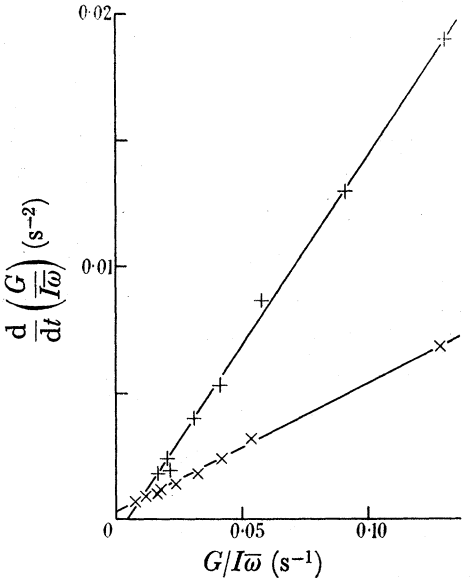

Figure 11. The decay of turbulence at subcritical velocities. +, can II C; ×, can I A.

(a) *The decay of turbulence at subcritical velocities*

At subcritical velocities ($\bar{\omega} < 0{\cdot}16$ rad/s) the rate of decay of turbulence is found to be independent of $\bar{\omega}$. This is illustrated in figure 11, which shows the rate of decay of turbulence as a function of turbulent intensity for all points for which $\bar{\omega} < 0{\cdot}16$ rad/s; it can be seen that the points for each disk system lie well on a single line, although they are derived from results for three different initial angular velocities. Apart from the fact that the straight lines of figure 11 do not pass quite through the origin, which may well be due to experimental error, the decay of turbulence appears to be exponential in this region; the time constants defined by the slopes of the lines, 6·7 s for can II C and 19·6 s for can I A, are almost exactly proportional to disk separation. This suggests that the dominant decay process occurs at the disk surfaces. If, for example, the vortex lines constituting the turbulence are considered as a set of particles moving independently with velocity v_L, and if these 'particles'

of vortex line are annihilated when they hit the disk surfaces, then the turbulence should decay according to the law

$$\frac{d\bar{\Omega}}{dt} = -\Omega\frac{v_L}{4d} = -\frac{\Omega}{t_0} \tag{18}$$

in a gap of width d. The experimental results agree with equation (18) if $v_L = 4{\cdot}6 \times 10^{-3}$ cm/s. A time-scale proportional to gap width has also been found by Vinen (1957*b*) for the final decay of the turbulence generated in a heat flow; Vinen's method of observation does not give the form of the decay, but the time scale observed in gaps of about 2 and 4 mm is certainly of the order of magnitude predicted by equation (18).

(*b*) *The growth and decay of strong turbulence*

For analysis of the values of $d\bar{\Omega}/dt$ for $\bar{\omega} > 0{\cdot}16$ rad/s to be practicable it is necessary to make a more specific assumption than equation (5); a natural assumption is that the time dependence of the turbulence can be considered as a balance of separate growth and decay processes. We shall therefore assume that

$$\frac{1}{\bar{\Omega}^x}\frac{d\bar{\Omega}}{dt} = f(\bar{\omega}) - g(\bar{\Omega}), \tag{19}$$

where the functions f and g, representing growth and decay, respectively, are to be determined. The parameter x is included so that a possible dependence of the rate of growth of turbulence on the existing turbulent intensity can be considered; if the turbulence is to grow in a finite time from a zero initial value we must choose $x < 1$. The results of the previous section show that $f(\bar{\omega})$ is negligibly small for $\bar{\omega} < 0{\cdot}16$ rad/s, and $g(\bar{\Omega})$ can therefore be determined directly from them for small values of $\bar{\Omega}$.

The curve of equilibrium turbulent intensity (broken curve in figure 7) can be specified by either $\bar{\Omega}_{eq.}(\bar{\omega})$ or $\bar{\omega}_{eq.}(\bar{\Omega})$, where $\bar{\Omega}_{eq.}$ and $\bar{\omega}_{eq.}$ satisfy the equations

$$f(\bar{\omega}_{eq.}) = g(\bar{\Omega}), \tag{20}$$

$$f(\bar{\omega}) = g(\bar{\Omega}_{eq.}), \tag{21}$$

since $d\bar{\Omega}/dt = 0$ in equilibrium. From equation (20) and the values of $g(\bar{\Omega})$ deduced from the results of the previous section $f(\bar{\omega})$ can be found for small values of $\bar{\omega}$. The functions f and g can then be determined for larger values of the argument in the following way. Equations (20) and (21) enable equation (19) to be written in the alternative forms

$$\frac{1}{\bar{\Omega}^x}\frac{d\bar{\Omega}}{dt} = g(\bar{\Omega}_{eq.}) - g(\bar{\Omega}) \tag{22}$$

$$= f(\bar{\omega}) - f(\bar{\omega}_{eq.}), \tag{23}$$

by means of which known values of $g(\bar{\Omega}_{eq.})$ or $f(\bar{\omega}_{eq.})$ can be combined with values of $d\bar{\Omega}/dt$ for $\bar{\omega} > 0{\cdot}16$ rad/s to give further values of $g(\bar{\Omega})$ or $f(\bar{\omega})$. If $\bar{\Omega} > \bar{\Omega}_{eq.}$ equation (22) is used to determine $g(\bar{\Omega})$, and then $f(\bar{\omega}_{eq.})$ is found from equation (20); if $\bar{\Omega} < \bar{\Omega}_{eq.}$ (i.e. $\bar{\omega} > \bar{\omega}_{eq.}$) equations (23) and (21) are used in a similar way. In order to obtain an experimental estimate of the initial rate of growth of turbulence it is assumed that $\bar{\Omega} = \omega_0$ at $t = 0$, i.e. that the vortex line due to uniform rotation can be regarded as an effective initial turbulent intensity; this assumption is probably not accurately true, since the initial array

of vortex line is regular rather than disordered, but it should enable the order of magnitude of the initial rate of growth to be estimated correctly.

The procedure described above has been applied to the experimental results so as to test the validity of equation (19) with $x = 0$ or $x = \frac{1}{2}$. It is found that the results can be fitted moderately well by either

$$\frac{\mathrm{d}}{\mathrm{d}t}\left(\frac{G}{I\bar{\omega}}\right) = f_1(\bar{\omega}) - g_1\left(\frac{G}{I\bar{\omega}}\right), \tag{24}$$

with $f_1(\bar{\omega}) = k_1\bar{\omega}^4$, $k_1 = 1{\cdot}0\,\mathrm{s}^2$, or

$$\left(\frac{I\bar{\omega}}{G}\right)^{\frac{1}{2}}\frac{\mathrm{d}}{\mathrm{d}t}\left(\frac{G}{I\bar{\omega}}\right) = f_2(\bar{\omega}) - g_2\left(\frac{G}{I\bar{\omega}}\right), \tag{25}$$

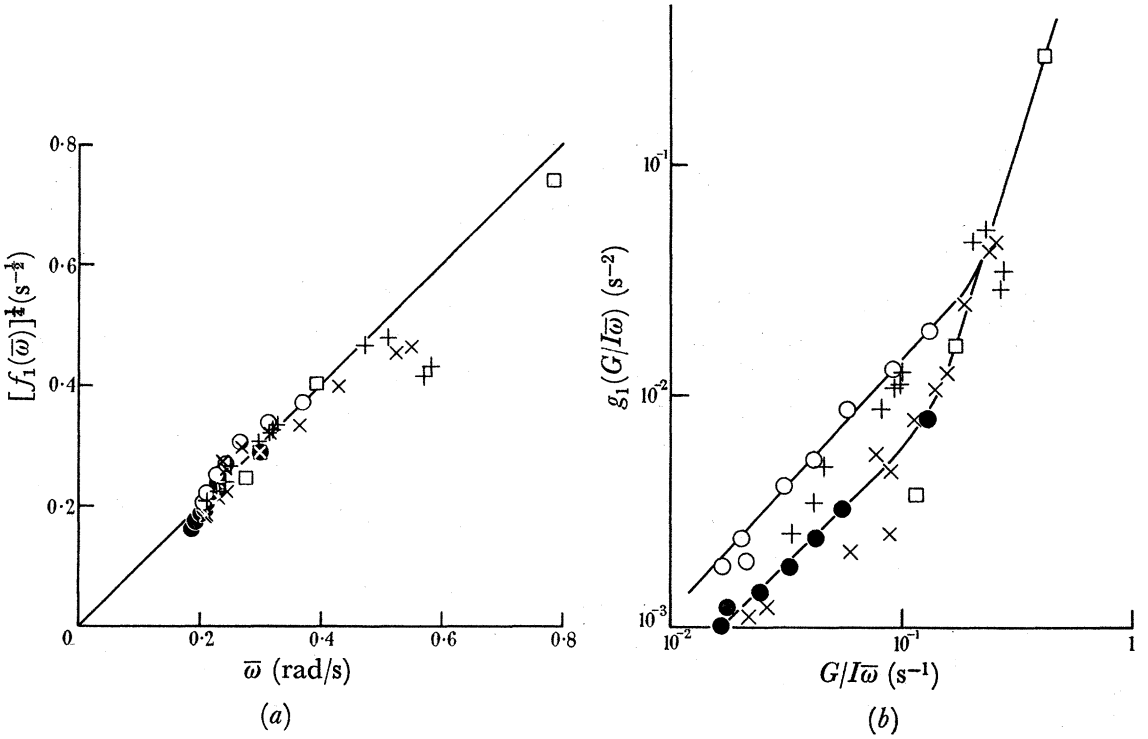

FIGURE 12. The functions f and g, which govern the growth and decay of turbulence. + ×, subcritical points for cans IIC and IA, respectively; ○ ●, supercritical points for cans IIC and IA, respectively; □, estimated from the initial rate of growth of turbulence in can IA.

with $f_2(\bar{\omega}) = k_2\bar{\omega}^3$, $k_2 = 1{\cdot}6\,\mathrm{s}^{\frac{3}{2}}$; the data illustrating equation (24) are shown in figure (12). It can be seen that the points are badly scattered, largely because they are derived from the experimental results by a numerical integration and a numerical differentiation. The results for the assumption $x = \frac{1}{2}$ are similar; the points fit together better in some respects and worse in others. At low turbulent intensities

$$g_1\left(\frac{G}{I\bar{\omega}}\right) = \left(\frac{G}{I\bar{\omega}}\right)^{\frac{1}{2}} g_2\left(\frac{G}{I\bar{\omega}}\right) = \frac{G}{I\bar{\omega}t_0}, \tag{26}$$

where the time constant t_0 is given by equation (18), but at high turbulent intensities the values of g for the two disk separations converge. It is interesting to note that for the turbulent intensity at which g begins to rise above the value given by equation (26) the mean spacing

between the vortex lines, calculated on the assumption of a circulation h/m round each line, is approximately equal to the disk separation. This is a very reasonable value for the turbulent intensity at which decay of turbulence in the body of the liquid begins to dominate decay on the disk surfaces.

It can be seen from figure 12 (*a*) that there is no significant evidence of any dependence of $f(\bar{\omega})$ on disk separation; this result, together with equation (26), should lead to different equilibrium turbulent intensities for the two disk systems at low velocities. For this reason the observed differences in equilibrium turbulent intensity around $\bar{\omega} = 0{\cdot}25$ rad/s (see, for example, figure 8) are thought to be genuine, although they are not outside the possible experimental error. A particularly interesting feature of figure 12 (*a*) is that there is no evidence of any sharp drop in $f(\bar{\omega})$ at the critical velocity; this suggests that there is still some turbulence below the critical velocity, the rapid fall in equilibrium turbulent intensity in a narrow velocity range being due to the change in behaviour of $g(\bar{\Omega})$ shown in figure 12 (*b*) and discussed above. In fact equation (24) gives $\bar{\Omega}_{\mathrm{eq.}} = k_1 t_0 \bar{\omega}^4$ at low velocities and equation (25) gives $\bar{\Omega}_{\mathrm{eq.}} = (k_2 t_0)^2 \bar{\omega}^6$. These results can be used to calculate the lifetime of a persistent current, which was found experimentally to be greater than 25 min for can II C (§ 3 (*b*)); equation (24) gives a calculated lifetime of 10 min and equation (25) 35 min. Therefore, if $x = 0$ (equation (24)), the rate of growth of turbulence in the subcritical region must be rather smaller than the rate given by the straight line of figure 12 (*a*).

We may also note that if the growth law of either of equations (24) or (25) is valid at high velocities, where the mutual friction is given by equation (17) and v_0 is negligible, then the decay law takes the limiting form

$$\mathrm{d}\bar{\Omega}/\mathrm{d}t = -\alpha\bar{\Omega}^2, \tag{27}$$

where $\alpha = 0{\cdot}78 \pm 0{\cdot}15$ if equation (24) is valid and $\alpha = 0{\cdot}67 \pm 0{\cdot}15$ if equation (25) is valid. This is precisely the form of the decay law for ordinary homogeneous turbulence,

$$\mathrm{d}u^2/\mathrm{d}t \doteqdot -u^3/l, \tag{28}$$

(Batchelor 1953), if the product of length scale l and velocity scale u is constant, as it should be for a turbulence consisting of vortex lines of constant circulation. Furthermore, equation (27) with (24) or (25) gives a time scale for the growth and decay of turbulence that is proportional to the acceleration time-scale, as was found in § 3 (*a*) for the experimental results at high speeds. It is probable, therefore, that equation (27) does indeed represent the decay of strong turbulence; the fact that the constant α is of the order of magnitude found in ordinary liquids provides some evidence that $\bar{\Omega}$ is equal to the mean angular velocity of the turbulence, as it should be according to the definition of equation (4).

The decay law of the turbulence is thus fairly well established, since it is very similar for equations (24) and (25). In order to decide which equation gives the best representation of the growth law of the turbulence we adopt a different approach which avoids the magnification of experimental inaccuracy inherent in computing experimental values of $\mathrm{d}\bar{\Omega}/\mathrm{d}t$; we compute torque-time curves for can I A by numerical integration of equation (24) or (25) together with the acceleration equation

$$\frac{1}{\bar{\omega}}\frac{\mathrm{d}\bar{\omega}}{\mathrm{d}t} = -\frac{G}{I\bar{\omega}}, \tag{29}$$

and compare the computed curves with the experimentally observed torque-time curves. For this purpose g is taken from equation (26) with $t_0 = 17{\cdot}5$ s (from the slope of the best straight line through the origin in figure 11) at low turbulent intensities, and at high turbulent intensities g is deduced from f with the aid of the experimental values of $\overline{\Omega}_{eq.}$ and equation (21). It is assumed, as before, that $\overline{\Omega} = \omega_0$ at $t = 0$ for retardation from a state of rotational equilibrium. The results of these computations are shown in figure 13. Curves

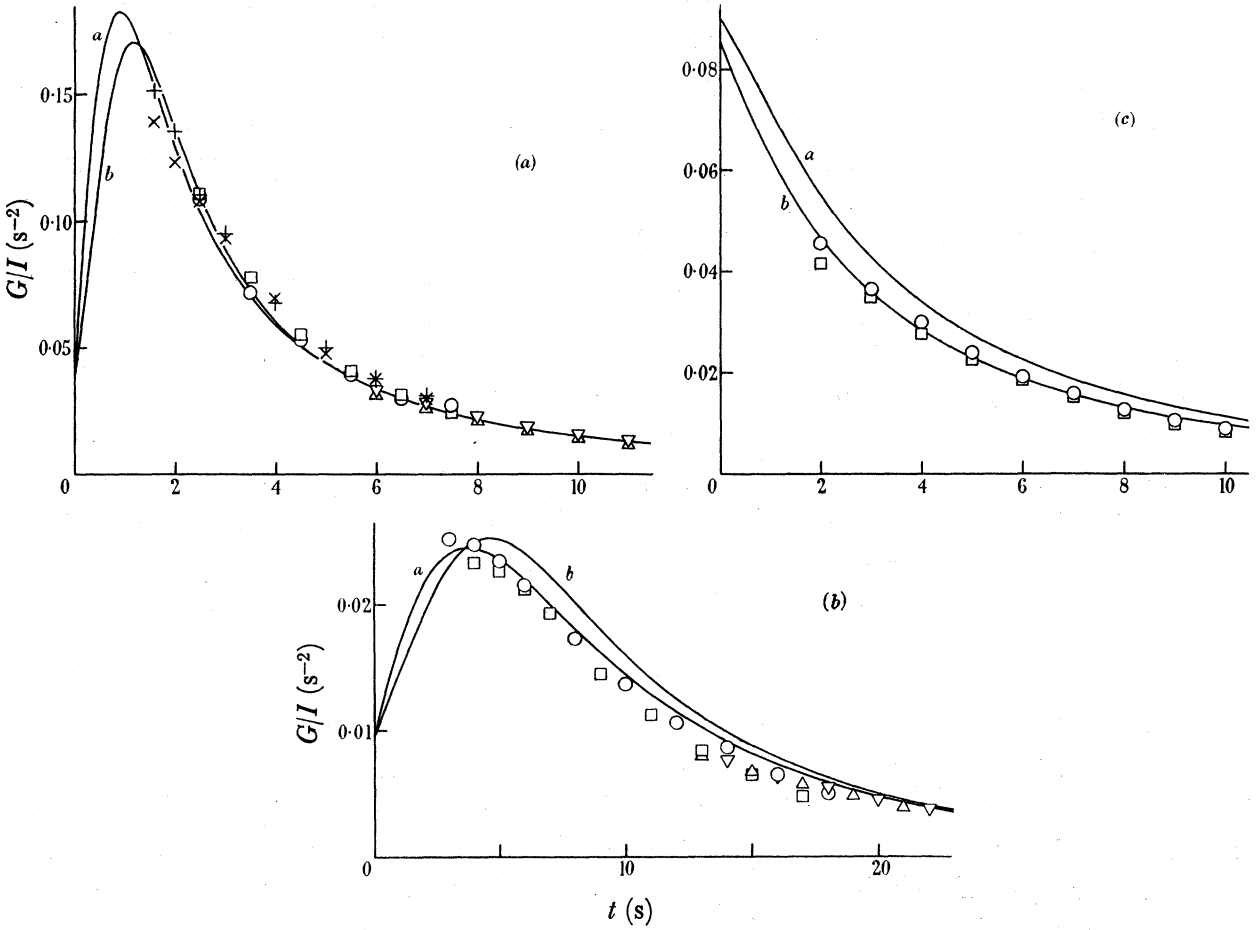

FIGURE 13. Comparison of calculated and observed retardation curves for can IA. (*a*) Retardation from equilibrium at 0·785 rad/s; (*b*) retardation from equilibrium at 0·393 rad/s; (*c*) retardation after 4 s rotation at 0·785 rad/s. The different experimental points represent repetitions of the experiment at various sensitivities; curves *a*, calculated from equations (24) and (29) ($x = 0$); curves *b*, calculated from equations (25) and (29) ($x = \frac{1}{2}$).

for retardation from a state of rotational equilibrium at 0·785 and 0·393 rad/s are shown in figures 13 (*a*) and (*b*); at the higher speed either $x = 0$ or $x = \frac{1}{2}$ fits the experimental results adequately, but at the lower speed only $x = 0$ (equation (24)) gives a sufficiently rapid initial rate of growth of turbulence. This result is not, however, decisive, since our assumption that the vortex lines due to uniform rotation can be adequately accounted for by taking $\overline{\Omega} = \omega_0$ at $t = 0$ may be in error. A better test is provided by the results for the acceleration process, which we have not yet considered in this section, since in this case $\overline{\Omega} = 0$ at $t = 0$. The main effect of the different initial conditions is to delay the acceleration process relative to the retardation process; this delay is predicted to be about 0·1 s if $x = 0$

and 0·6 s if $x = \frac{1}{2}$ (for $\omega_0 = 0{\cdot}785$ rad/s). These predictions can be compared with experiment by computing the retardation curves to be expected when rotation is stopped after 4 s of acceleration; the result is shown in figure 13 (*c*), and clearly favours the assumption $x = \frac{1}{2}$ (equation (25)). The curve for $x = 0$ lies everywhere higher because the initial stages of acceleration are more rapid in this case, so that the superfluid acquires more angular momentum in a given time. We may remark that this dependence of the difference between acceleration and retardation on the form of the growth law of turbulence means that no reliable estimate of the constant B can be made by comparing the experimental results for acceleration and retardation (see § 3 (*c*)).

Thus, the retardation results favour the assumption $x = 0$ and the acceleration results favour $x = \frac{1}{2}$. More explicitly, the rapid initial growth of turbulence during retardation suggests that the rate of growth is substantially independent of the existing turbulent intensity; but the delay of acceleration relative to retardation, and also the observed lifetime of a persistent current (see above), indicate that the rate of growth is reduced at very low turbulent intensities. It thus seems probable that the dependence of the rate of growth of turbulence on turbulent intensity is too complicated to be represented by the single parameter x of equation (19); the results are best represented by equation (24) ($x = 0$), except for a decrease in the rate of growth at small turbulent intensities, the precise form of which cannot be determined from the data available. This growth law is probably not applicable to all flows, however, since experiments on mutual friction in a heat flow (Vinen 1957*c*) indicate a rather different dependence of growth rate on turbulent intensity; further experiments are needed to clarify the situation.

6. Conclusion

A self-consistent account of the angular acceleration of helium II has been given in terms of a mutual friction due to the presence of vortex lines in the superfluid. Values of the equilibrium turbulent intensity in a steady flow have been obtained, and they are in agreement with values deduced from other experiments; these results, and those on the growth and decay of turbulence, provide quantitative data which any satisfactory theory of superfluid turbulence must explain.

I am grateful to Dr D. Shoenberg, F.R.S., for his constant encouragement and for advice on the presentation of this paper, to him and to Dr J. Ashmead, Dr D. V. Osborne, Dr A. B. Pippard, F.R.S. and Dr W. F. Vinen for many helpful discussions, and to Mr F. T. Sadler and Mr W. A. R. Whitmore for the construction of apparatus. The work was initially supported by a maintenance grant from the Department of Scientific and Industrial Research, and its completion was made possible by the award of a Research Fellowship at Emmanuel College, Cambridge and a Senior Studentship of the Royal Commission for the Exhibition of 1851.

References

Andronikashvili, E. L. 1952 *J. Exp. Theor. Phys. U.S.S.R.* **22**, 62.
Atkins, K. R. 1950 *Proc. Roy. Soc.* A, **203**, 119.
Atkins, K. R. 1951 *Proc. Phys. Soc.* A, **64**, 833.
Batchelor, G. K. 1953 *The theory of homogeneous turbulence*, chap. VI. Cambridge University Press.
Bowers, R. & Mendelssohn, K. 1950 *Proc. Roy. Soc.* A, **204**, 366.

PHILOSOPHICAL TRANSACTIONS OF THE ROYAL SOCIETY A MATHEMATICAL, PHYSICAL & ENGINEERING SCIENCES

Carslaw, H. S. & Jaeger, J. C. 1947 *The conduction of heat in solids*, p. 83. Oxford University Press.
Donnelly, R. J., Chester, G. V., Walmsley, R. H. & Lane, C. T. 1956 *Phys. Rev.* **102**, 3.
Donnelly, R. J. & Penrose, O. 1956 *Phys. Rev.* **103**, 1137.
Feynman, R. P. 1955 *Progress in low temperature physics* (ed. C. J. Gorter), vol. 1, chap. II, p. 36. Amsterdam: North Holland Publishing Co.
Gorter, C. J. & Mellink, J. H. 1949 *Physica*, **15**, 285.
Hall, H. E. 1955 *Conférence de physique des basses températures*, p. 63. Paris.
Hall, H. E. & Vinen, W. F. 1955 *Phil. Mag.* **46**, 546.
Hall, H. E. & Vinen, W. F. 1956*a* *Proc. Roy. Soc.* A, **238**, 204.
Hall, H. E. & Vinen, W. F. 1956*b* *Proc. Roy. Soc.* A, **238**, 215.
Heikkila, W. J. & Hollis-Hallett, A. C. 1955 *Canad. J. Phys.* **33**, 420.
Hollis-Hallett, A. C. 1952*a* *Proc. Roy. Soc.* A, **210**, 404.
Hollis-Hallett, A. C. 1952*b* Thesis, University of Cambridge.
Hollis-Hallett, A. C. 1953 *Proc. Camb. Phil. Soc.* **49**, 717.
Townsend, A. A. 1956 *The structure of turbulent shear flow*, chap. 12. Cambridge University Press.
Vinen, W. F. 1957*a* *Proc. Roy. Soc.* A, **240**, 114.
Vinen, W. F. 1957*b* *Proc. Roy. Soc.* A, **240**, 128.
Vinen, W. F. 1957*c* *Proc. Roy. Soc.* A, **242**, 493.

PHILOSOPHICAL TRANSACTIONS OF THE ROYAL SOCIETY A MATHEMATICAL, PHYSICAL & ENGINEERING SCIENCES

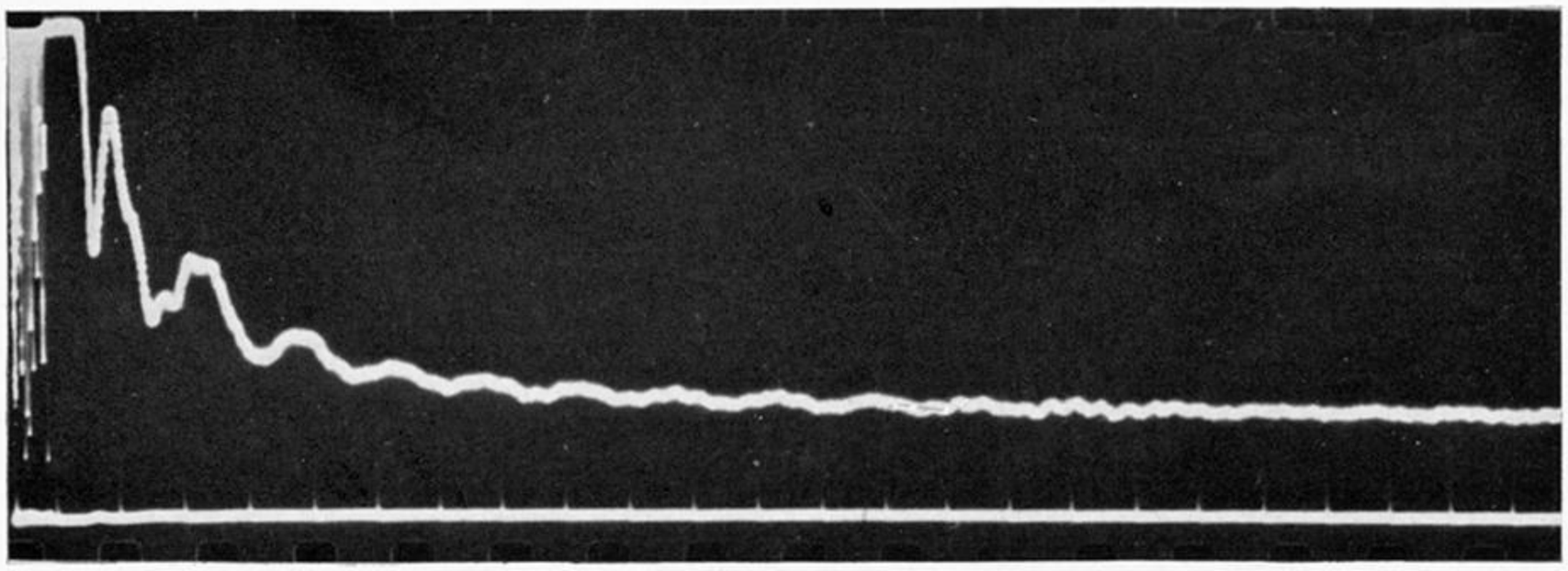

	ω_0	width of film
(*a*)	0·785 rad/s	≈ 0·4 dyn cm

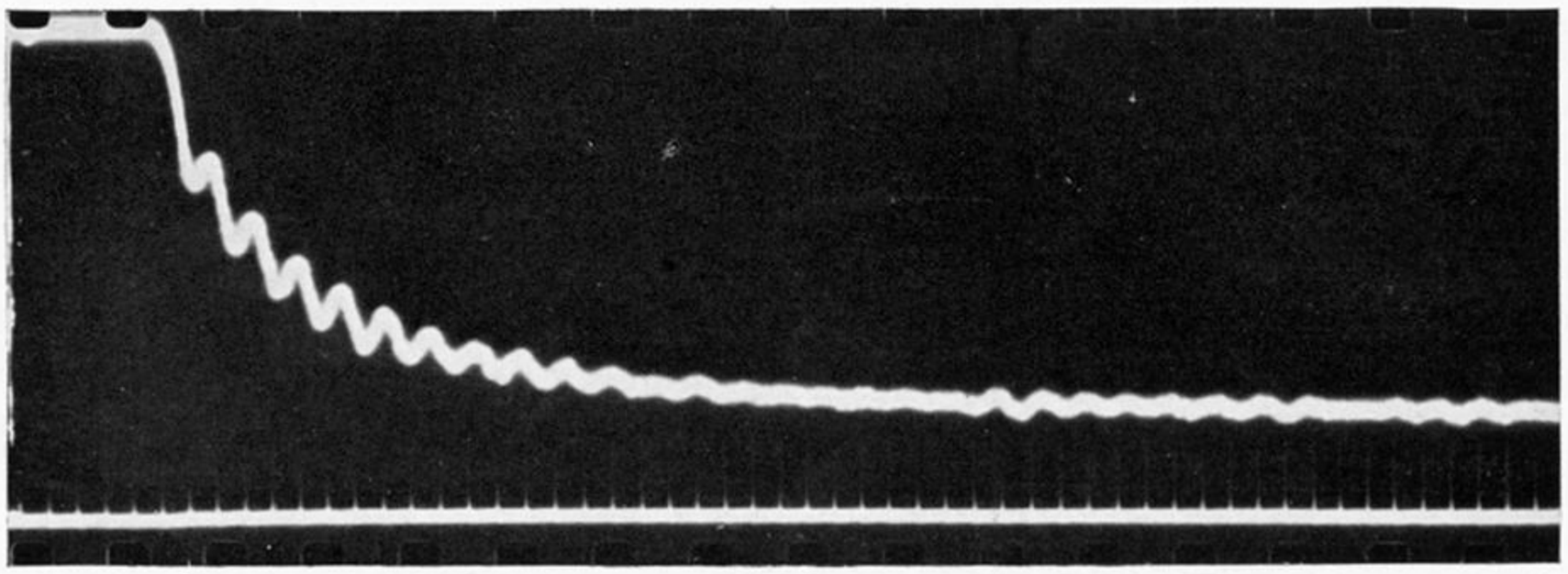

(*b*)	0·785	≈ 0·04

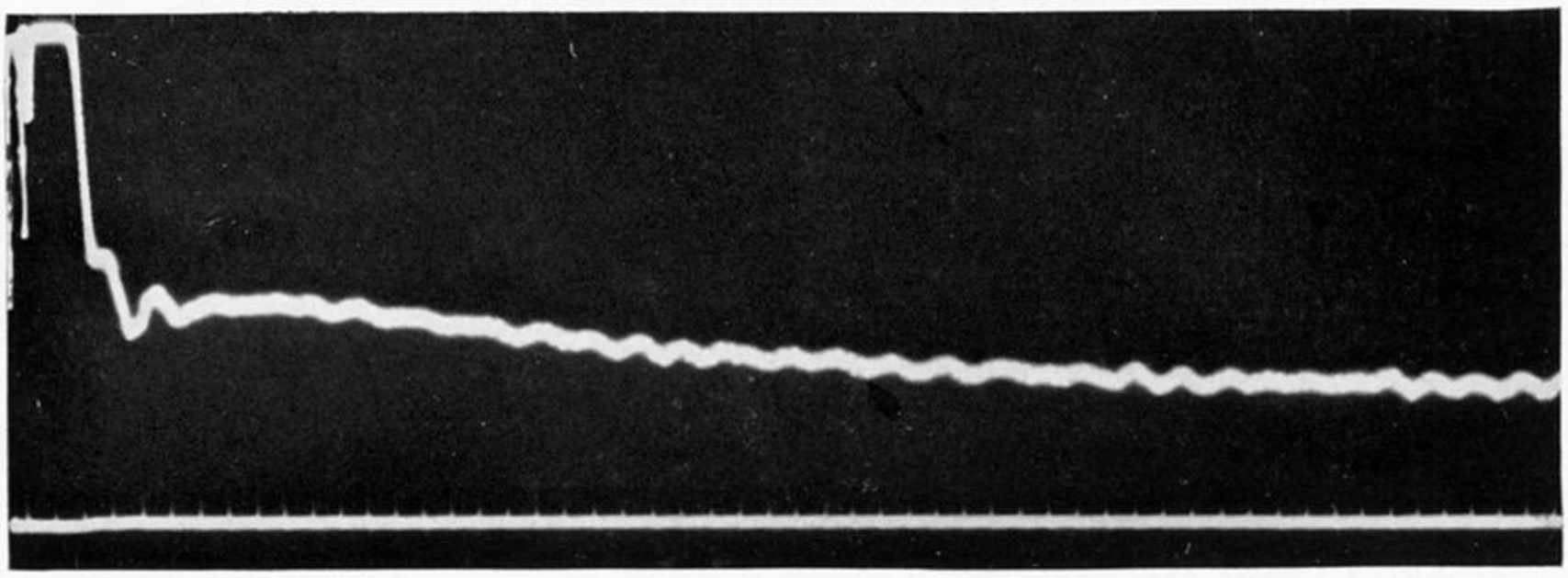

(*c*)	0·196	≈ 0·02

FIGURE 2. Torque-time curves for retardation of the liquid in can OA (upper trace) with timing marks at 1s intervals (lower trace).

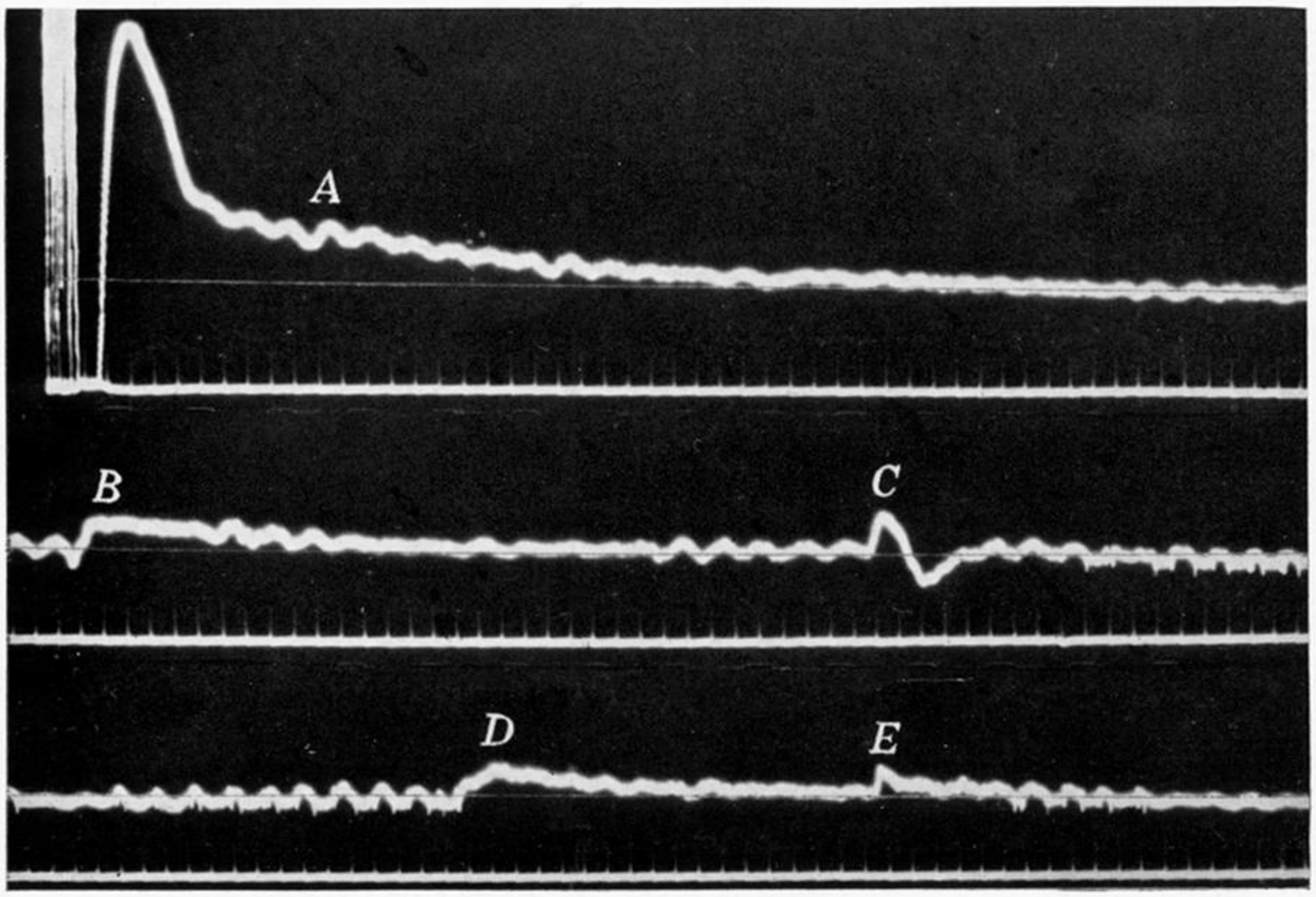

FIGURE 5. The torque pulses observed with can II C during retardation from an initial speed of 0·196 rad/s.

(*Facing p.* 363)